STUDIES ON SOLAR-TERRESTRIAL PHYSICS IN RUSSIA: 2010-2011

GELIY ZHEREBTSOV

RUSSIAN REPRESENTATIVE IN SCOSTEP,
CHAIRMAN OF THE RUSSIAN "SUN-EARTH" COUNCIL

GALINA KOTOVA

EXECUTIVE SECRETARY
OF THE RUSSIAN "SUN-EARTH" COUNCIL
kotova@iki.rssi.ru

Main meetings:

- *The third symposium on solar-terrestrial physics in Russia, devoted to 50th anniversary of the Institute of Solar-Terrestrial Physics SB RAS was held in Irkutsk on 28 – 30 June 2010.*
- *All-Russia annual conference "Solar and Solar-Terrestrial Physics" (St.Petersburg, Pulkovo observatory)*
  - *2009: July 5-11*
  - *2010: October 3-9*
  - *2011: October 3-9*
- *Annual international seminar in Polar Geophysical Institute, Apatity*
  - *2009: March 3-6*
  - *2010: March 2-5*
  - *2011: March 1-4*
- *"JENAM-2011. European Week of Astronomy and Space Science". The symposium S3: "The Sun: New Challenges" (St.Petersburg, 2011, July 4-8)*
- *The 9th Russian-Chinese Conference on Space Weather (Irkutsk, ISTP SB RAS 23–27 June, 2009)*
- *The 9th Russian-Mongolian Conference on Astronomy and Geophysics (Irkutsk, ISTP SB RAS, 10-13 October 2011)*
- *Baikal Young Scientists' International School*
  - *2009: September 7-12 "Helio and Geophysical Researches"*
  - *2011: September 19-24 "Physical processes in space and circumterrestrial environment"*

1. SOLAR PHYSICS

Results obtained from ground-based observations.

Data are mainly collected by:

- Central Astronomical Observatory of Russian Academy of Sciences at Pulkovo (CAO RAN, http://www.gao.spb.ru):
  - Kislovodsk Solar Mountain Station
  - Pulkovo Horizontal solar telescope
  - The Big Pulkovo radio telescope
- The Special Astrophysical Observatory of Russian Academy of Sciences (Nizhny Arhyz, http://www.sao.ru/):
  - RATAN 600
- Institute of Solar-Terrestrial Physics of Russian Academy of Sciences, Siberian Branch (ISTP RAS, http://iszf.irk.ru/)
  - Sayan Solar observatory
  - Siberian solar radio telescope
  - Baikal astrophysical observatory
- Radiophysical research institute (NIRFI, http://solar.nirfi.sci-nnov.ru/RAS_Zimenki/)
  - Zimenki Radio Astronomical Station

Center for analysis of multiwave solar observations by RATAN-600.

http://www.spbf.sao.ru/

The center is created on the basis of St.-Petersburg branch of the Special Astrophysical Observatory of RAS.

The development of spectral receiver complex for solar radio emission study by large radio telescope RATAN-600 was continued. The frequency range covered the interval of 0.75 - 18 GHz with resolution of ~1 % in 112 frequency channels. The instant records of all frequency channels were realized. The wide and detail spectra of intensity and polarization in combination with large effective surface of the radiotelescope give new opportunities to study fine height structures in solar atmosphere. The regular solar observations are treated automatically and are represented on the site http://www.spbf.sao.ru/prognoz

Contact V.M.Bogod and S.Tokhchukova (vbog@sao.ru)

Creation of data center for radioastronomical monitoring of solar activity

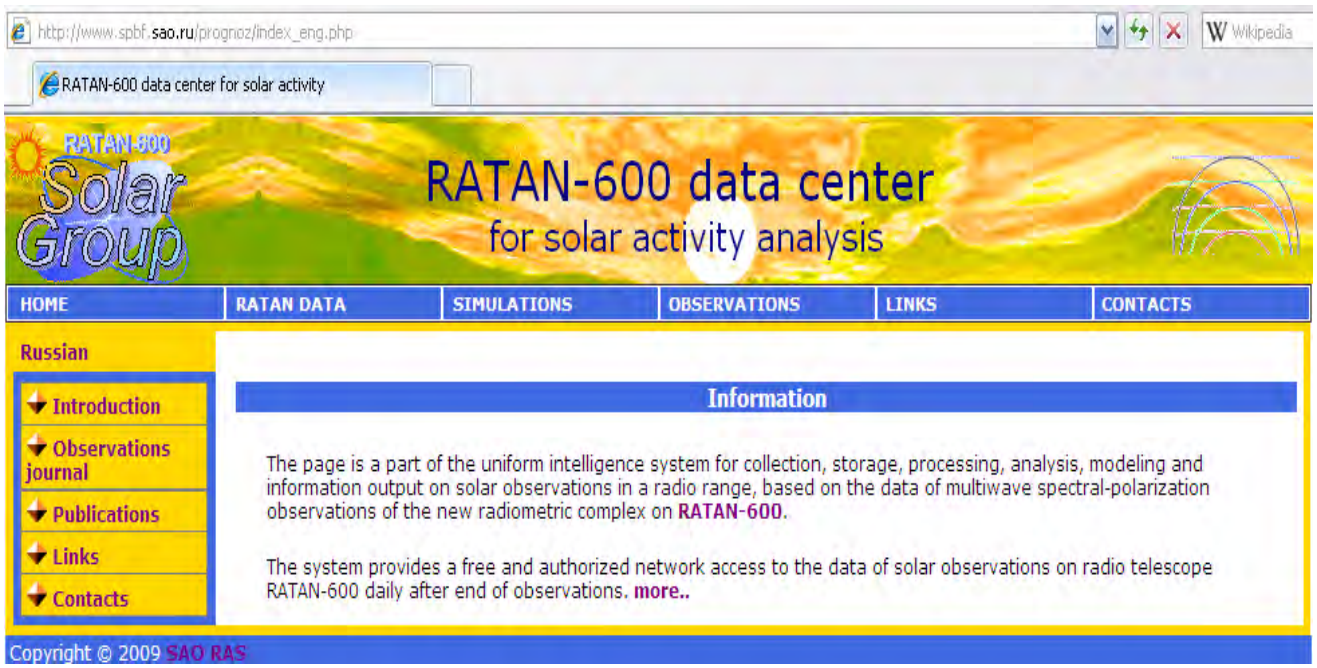

Now the wide range solar radio spectrograph is using in regular observations of the Sun with the help of large radiotelescope RATAN-600.

PARAMETERS:
Bandwidth – 0.75 GHz – 18.2 GHz;
Spectral resolution - 1%;
Recording speed - 2.5 mlsec/spectrum,
Sensitivity- 0.003 s.f.u.;
Number of recording channels – 224
RH polarizations - 112 channels
LH polarizations - 112 channels

Daily presentation of the data on site http://www.spbf.sao.ru/prognoz/

7.02.2010 6.02.2010 5.02.2010

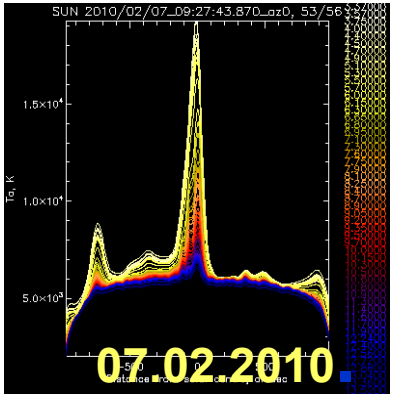

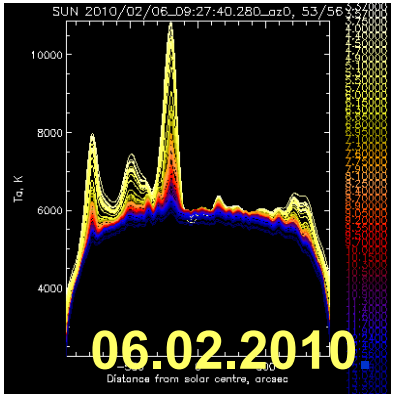

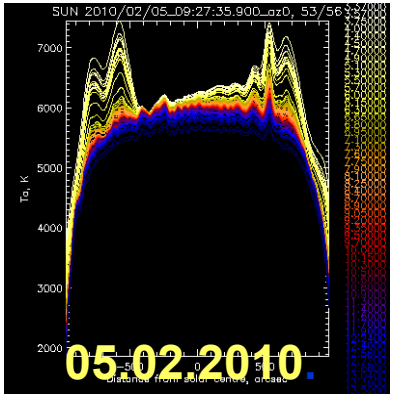

All the multiwave data are presented for free using. Full treatment of the data is possible.

Contact S. Tokhchukova (stokh@mail.ru)

Study of fine spectral features of polarized emission at pre-flare stage of active regions.

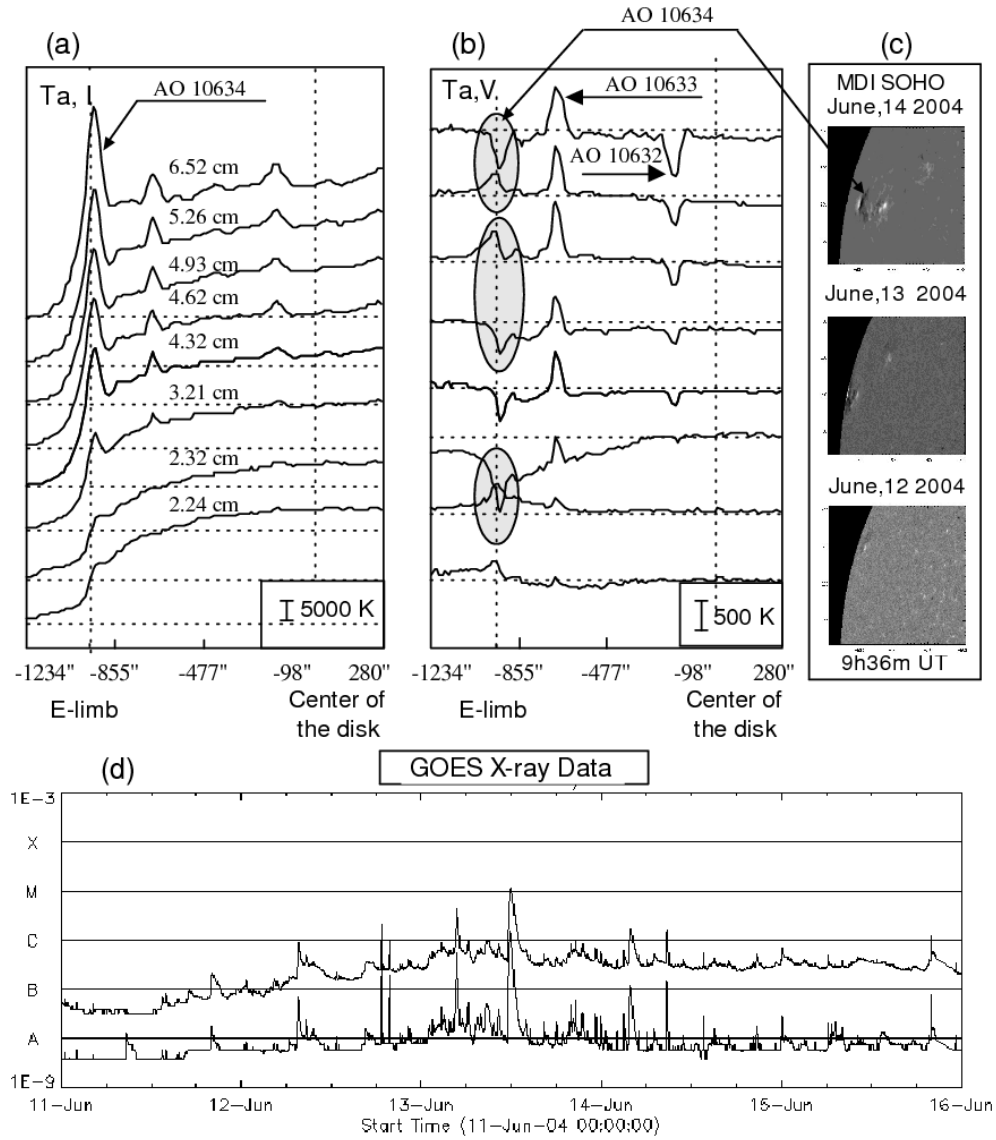

On the basis of multi-wavelength observations made with the one-dimensional RATAN-600 radio telescope, we study the inversion of the circular polarization in the solar microwave emission at different frequencies.

The inversion is detected in the emission of flare-producing active regions (FPAR) at various stages of their development, starting from the pre-flare stage.

On the Figure:

a)Intensity scans of the Sun at different wavelengths,
b)Polarization scans with polarization inversions (ovals)
c)Appearance of the active region on the disk
d)Flare activity of AR according GOES-satellite

Contact V.M.Bogod (vbog@sao.ru)

Modernization of the Siberian Solar Radio Telescope (SSRT)

The 10-antenna prototype of multiwave radioheliograph was developed in the course of modernization of the Siberian Solar Radio Telescope (SSRT). The frequency band is 4-8 GHz. The testing results showed that the used technologies provided the planned parameters of the radioheliograph.

Antennas of the prototype as a part of SSRT

Contact A.T. Altyntsev
altyntsev@iszf.irk.ru

Missions under development

INTERHELIOPROBE

http://www.izmiran.ru/projects/space/INTERHELIOPROBE/

The mission is aimed at the study of the inner heliosphere and the Sun. The gravity-assisted maneuvers at Venus can be used for inclining the SC orbit to the ecliptic plane and conducting out-of-ecliptic observations of the Sun. The mission scientific payload will comprise the instruments for remote observations of the Sun (X-ray telescope-spectrograph, coronagraph, magnetograph, and photometer) and in-situ measurements in the heliosphere (magnetometer, solar-wind electron analyzer, plasma analyzer, analyzer of solar neutrons, detector of charged particles, gamma-ray spectrometer, X-ray spectrometer, and wave complex).

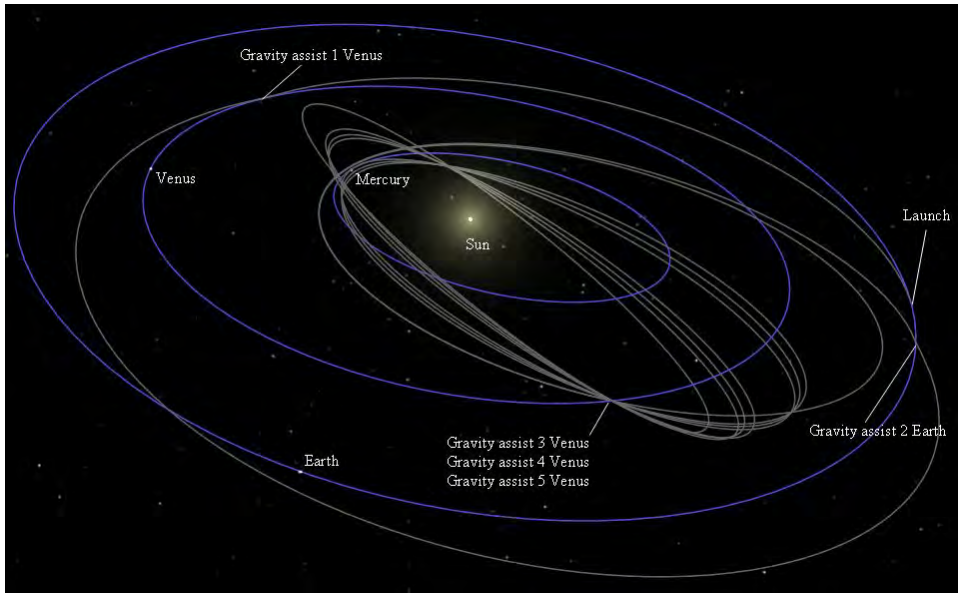

Interhelioprobe ballistic scheme.

Contact V.D.Kuznetsov (kvd@izmiran.ru)

Planned space missions

Polar Ecliptic Patrol

http://www.izmiran.ru/projects/space/PEP/

The mission is aimed at the study of the global pattern of solar activity, including its manifestations in the heliosphere and near-Earth space. The mission will comprise two small satellites. By gravity-assisted maneuvers at Venus, the satellites will be placed on heliocentric orbits inclined to the ecliptic plane at an angle to each other at distances about 0.5 AU from the Sun. The satellites on the orbits will be shifted about one another by a quarter of a period (one period is about 130 days). S*imultaneous monitoring* of the near-ecliptic and polar regions planned to be carried.
Stage A started in 2009, will be devoted to developing the details of the ballistic characteristics of the mission, its scientific tasks and instruments, and the tentative outward appearance of the spacecraft.

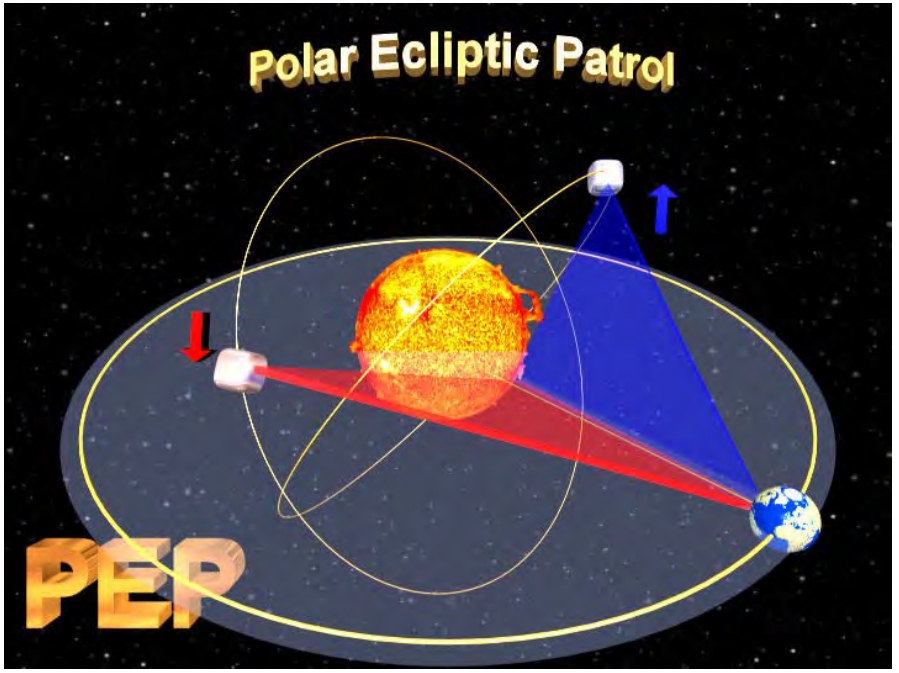

Ballistic scheme of the Polar Ecliptic Patrol.

Contact V.D.Kuznetsov (kvd@izmiran.ru)

The element abundances in the coronal plasma as inferred from the CORONAS-F/RESIK data

The analysis of numerous spectra of the solar X-ray continuum in the range of 1-7 A obtained with the CORONAS-F/RESIK instrument made it possible to determine the true flux of the solar continuous X-ray emission for the solar flares recorded in the period 2002-2003 and to estimate the abundances of rare elements, such as argon, potassium, and chlorine, in the solar corona. The method used to determine the element abundances is illustrated in the figure.

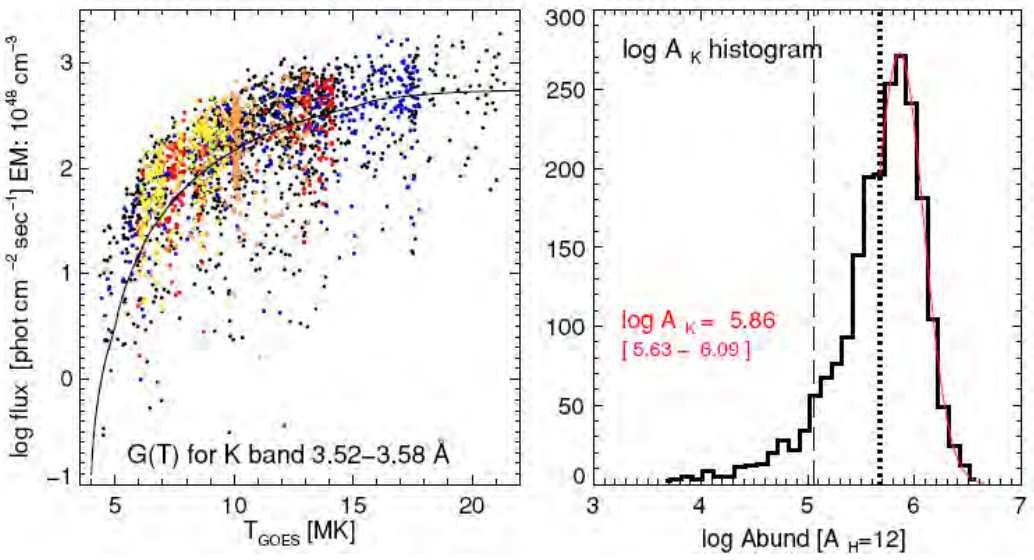

Left: flux of Kxviii *w* line (including unresolved dielectronic satellites) normalized to an emission measure of 10^{48} cm^{-3} (derived from *GOES*) plotted against T_{GOES}.
Right: number distribution of estimates of the deduced K abundance. The peak of the distribution corresponds to a K abundance of log*A*(K) = 5.86, with half-width corresponding to the range 5.63–6.09. The previous coronal (flare) abundance estimate of Doschek et al. (1985) is shown with the dotted vertical line, the photospheric estimates of Lambert & Luck (1978) and Takeda et al. (1996) by the dashed vertical line.

1.K.J.H.Phillips, J.Sylwester, B.Sylwester, V.D.Kuznetsov. The solar X-ray continuum measured by RESIK. Astrophys. J., ***711,*** *Issue 1, pp. 179-184, 2010.*
2. B.Sylwester, Kenneth J. H. Phillips, J.Sylwester, V.Kuznetsov. The Solar Flare Chlorine Abundance from RESIK X-ray Spectra. Astrophys. J., 738, 49, 2011.

Contact J.Sylwester and V.D.Kuznetsov (kvd@izmiran.ru)

Heating of the solar corona

A mechanism was proposed to account for the heating of the solar corona. The mechanism is based on the development of instabilities and dissipation of MHD waves propagating in the lower corona against the heat flow. It was shown that, under such conditions, a strong wave interaction takes place in the temperature-anisotropic plasma resulting in the development of instabilities.

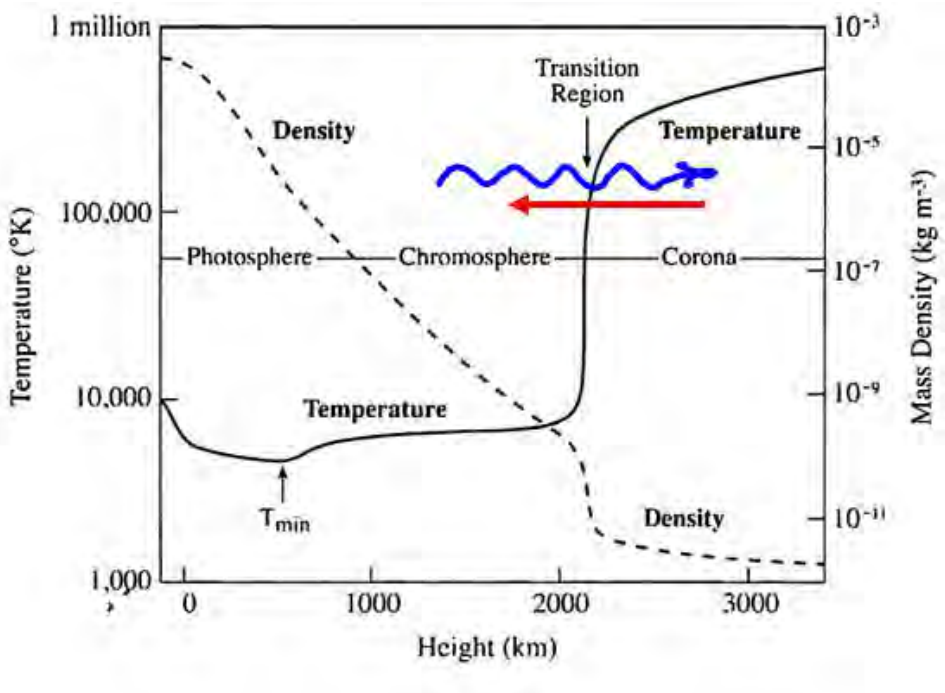

Wave propagation in the lower corona against the heat flow accompanied by the development of instabilities and wave dissipation

Periodic mirror instabilities of slow MHD waves can develop in the weak magnetic fields (B <1 G) and oscillatory ion-acoustic instabilities, in the strong ones (B >10 G). The determined instability growth rates and the temporal and spatial scales of the development and decay of the oscillatory instability suggest that the instabilities under consideration may contribute significantly to the energy balance of the corona and can be regarded as large-scale energy source in the wave mechanism of the corona heating. The model allows interpretation of the process as a self-consistent system; i.e., the wave interaction, development of instabilities, and wave dissipation occur owing to the heat counter flow, while the latter exists owing to the wave dissipation.

Contact V.D.Kuznetsov (kvd@izmiran.ru)

V.D.Kuznetsov, N.S.Dzhalilov. Anisotropic MHD Model and Some Solutions. Fizika Plazmy, v. 36, № 9, p.843-848, 2010. (V.D.Kuznetsov, N.S.Dzhalilov. Anisotropic MHD Model and Some Solutions/ Plasma Physics Reports, 2010, Vol. 36, No. 9, pp. 788–793).

Coronal Holes and High-Speed Solar Wind Streams

It was established that coronal holes (CH) on the Sun are very much similar to sunspots in their structure and play the same organizing role in the corona as the sunspots do in the photosphere. The solar wind originates in coronal holes at relatively low altitudes. The speed of the outflowing solar wind streams depends equally on the area of coronal holes and on their contrast. This fact allows us to relate the directly observed quantities, which can be used for the short-term forecast of geophysical disturbances.

A comparison of the CH photometric and magnetic structure has revealed that :

the darkest part of CH corresponds to the brightness less than 0.25 and, on the whole, the brightness is less than 0.5 of the mean solar brightness over the year under discussion;

the darkest part of CH corresponds to the maximum field strength;

the darkest part of CH corresponds to the region where the departure of field lines from the radial direction does not exceed 20°, while outside the darkest part, they can be strongly non-radial;

the CH as a whole is located in a unipolar field region;

With an adequate choice of the photometric boundaries, the CH area and brightness display a fairly high correlation with the solar wind velocity.

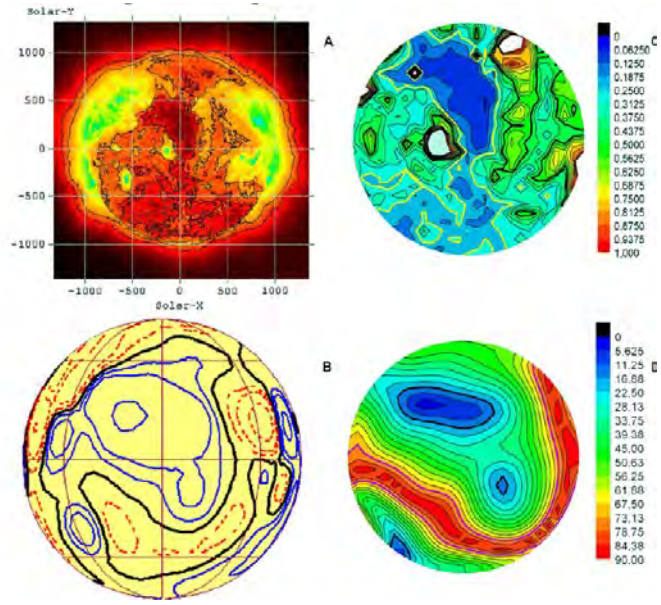

Comparison of the photometric and magnetic structure of a coronal hole. Panel A displays the original SOHO/EIT image with the contour lines at RL = 4 and RL = 8; panel B shows the structure of the radial magnetic field at 1.1*R*. The solid blue lines denote the positive polarity, and the red ones, the negative polarity. Panel C displays the brightness structure. The thick yellow and black lines outline the CH boundaries at the brightness level lower than 0.25 and 0.5 of the mean solar brightness, respectively. Panel D shows the departure of the field lines from the radial direction at 1.1*R*. The thick black and yellow lines bound the regions with deviation <20° and < 75°, respectively.

V.N.Obridko (IZMIRAN), B.D.Shelting (IZMIRAN), Solar Physics, 2011,270, 297-310

Contact V.N. Obridko
(obridko@izmiran.ru)

Magnetohydrostatical model of coronal hole

A model of coronal hole (CH) is proposed, which considers it to be an axially symmetric magnetic feature in magnetohydrostatic equilibrium with the environment (Fig.2). The model is valid for the lower corona (from the transition layer up to a few hundreds of km). It is shown that the structure of sunspots and that of coronal holes are identical in many respects.

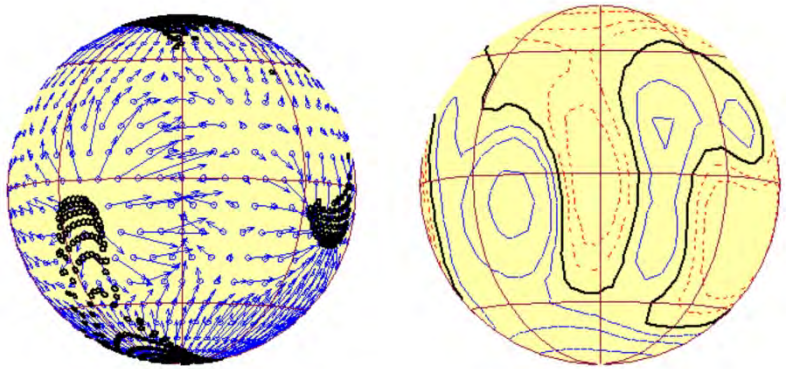

Fig.1 The maps of the solar magnetic field at the height of 1.1 $R_{\odot}$.

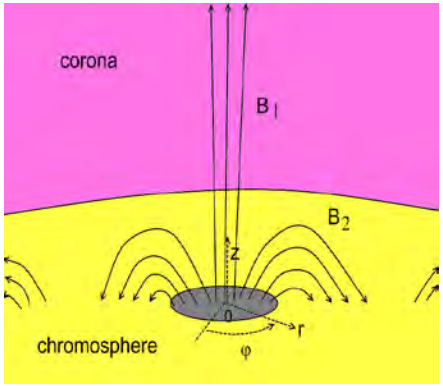

Fig. 2. A scheme of CH magnetic configuration

Fig.1 represents typical maps of solar magnetic field at the height of 1.1 $R_{\odot}$. On the left panel, the blue arrows denote the magnitude and direction of the transversal magnetic field, and the black circles show the footpoints of open field lines corresponding to the location of CH on the given day. One can see that equatorial coronal holes are located at the convergence or divergence of the field lines. A similar behavior of the field lines is observed in the sunspot penumbra. Like in sunspots, the flow of matter is canalized along the divergent field lines.

V.N.Obridko, A.A.Solovyev, Astron. Zh. 2011, 88, №12, 1-12.

Contact V.N. Obridko
(obridko@izmiran.ru)

Emergence of photospheric magnetic fields in a developing active region

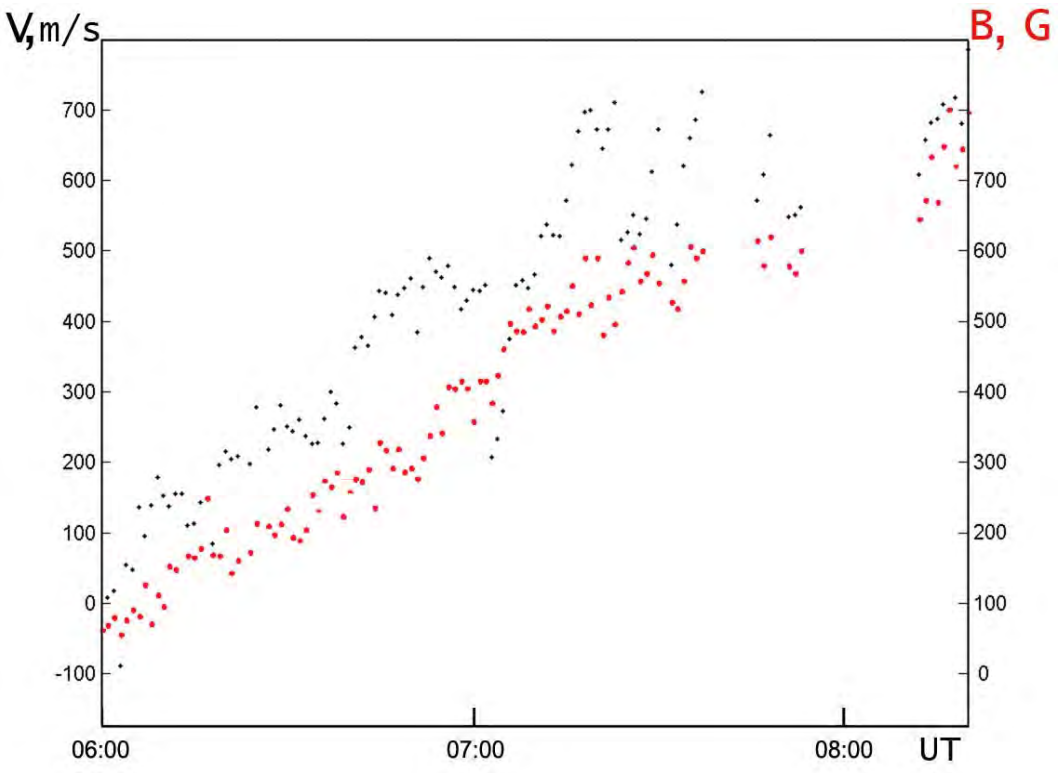

A direct relationship is found between the matter-downflow velocity ***V*** in the area of the forming sunspot and the growth in the strength of the longitudinal magnetic field ***B***.

The results concerning this point provide no evidence that any powerful MHD mechanism acts during the formation of a sunspot. It may be that the pore comes up from the subphotospheric levels, and the enhancement of the downflow is due to the gas rarefaction in the forming spot.

Contact V. Grigor'ev,
(vgrig@iszf.irk.ru)

V. M. Grigor'ev, L. V. Ermakova, and A. I. Khlystova
Astronomy Reports, 2011, 55, No. 2, pp. 163–173, 2011.

North–South Asymmetry in Sunspot Formation, Mean Sunspot Latitudes, and the Butterfly Diagram during Maunder minimum

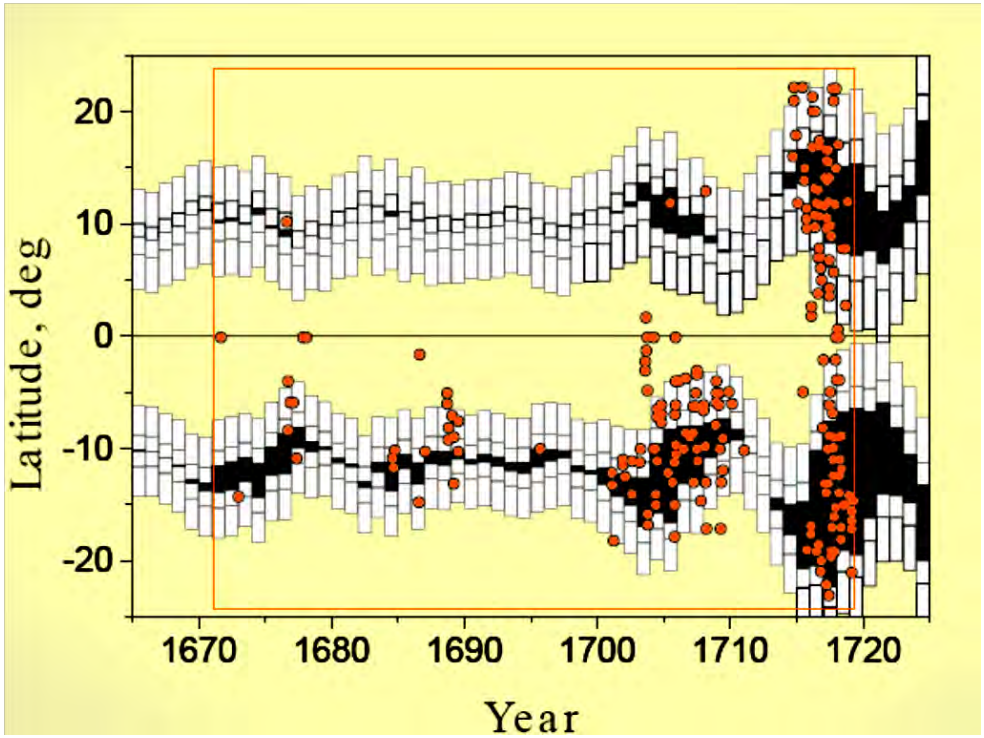

Model butterfly diagram in the Maunder minimum of solar activity (dark areas) and a comparison with the observations by Picard and de la Hire of 1671–1718 (orange circles). The vertical rectangles show 1σ and 3σ confidence intervals for the model in latitude.

DPS (Decomposition in pseudo-Phase Space) approach (*Nagovitsyn et al, Solar Phys.* ***224****, 2004*) to reconstructing solar activity in the past basing on Takens' theorem is used to study its space-time evolution. It is shown that we can now reconstruct not only the general level of solar activity on long timescales, but also particular aspects of its development: sunspot dominance in either hemisphere, the drift and latitude spread of the sunspot-formation zone, and features in the spatial distribution of the activity at specific epochs, such as the Maunder minimum.

Contact Yu.A. Nagovitsyn
(nag@gao.spb.ru)

Nagovitsyn Yu.A. et al, Astronomy Reports ***54****, 2010.*

Super Fast and Quality Azimuth Disambiguation

The possibility of fast and quality azimuth disambiguation of vector magnetogram data regardless of location on the solar disc is shown. The new Super Fast and Quality (SFQ) code of disambiguation is tried out on well-known models of Metcalf et al. (2006), Leka et al. (2009) and artificial model of fixed configuration AR 10930 (Rudenko et al., 2010). We make comparison of Hinode SOT SP vector magnetograms of AR 10930 disambiguated with three codes: SFQ, NPFC (Georgoulis, 2005), and SME (Rudenko et al., 2010). We exemplify the SFQ disambiguation of SDO/HMI measurements of the full disc. The preliminary examination indicates that the SFQ algorithm provides better quality than NPFC and is comparable to SME. In contrast to other codes, SFQ supports relatively high quality of results regardless of the magnetogram proximity to the limb (when being very close to the limb, it is efficient unlike all other algorithms).

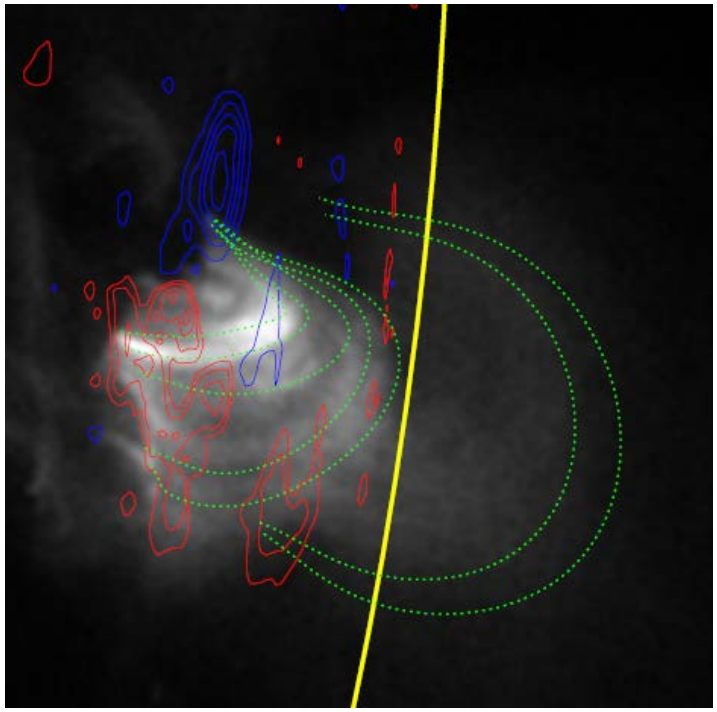

Field lines of the nonlinear force-free fields. Background is the X-ray image from *Hinode* XRT (17 December 2006 0:24:20.5 UT) with changed contrast. Contour lines are distribution of the calculated normal field component; yellow line is the limb.

Rudenko, G. V.; Myshyakov, I. I. Gauge-Invariant Helicity for Force-Free Magnetic Fields in a Rectangular Box, Solar Physics, Volume 270, Issue 1, pp.165-173, 2011.

Contact A.T. Altyntsev
altyntsev@iszf.irk.ru

Solar dynamo model

Numerical model for solar dynamo was developed that reproduces all basic features of global magnetic field dynamics over the solar cycles.

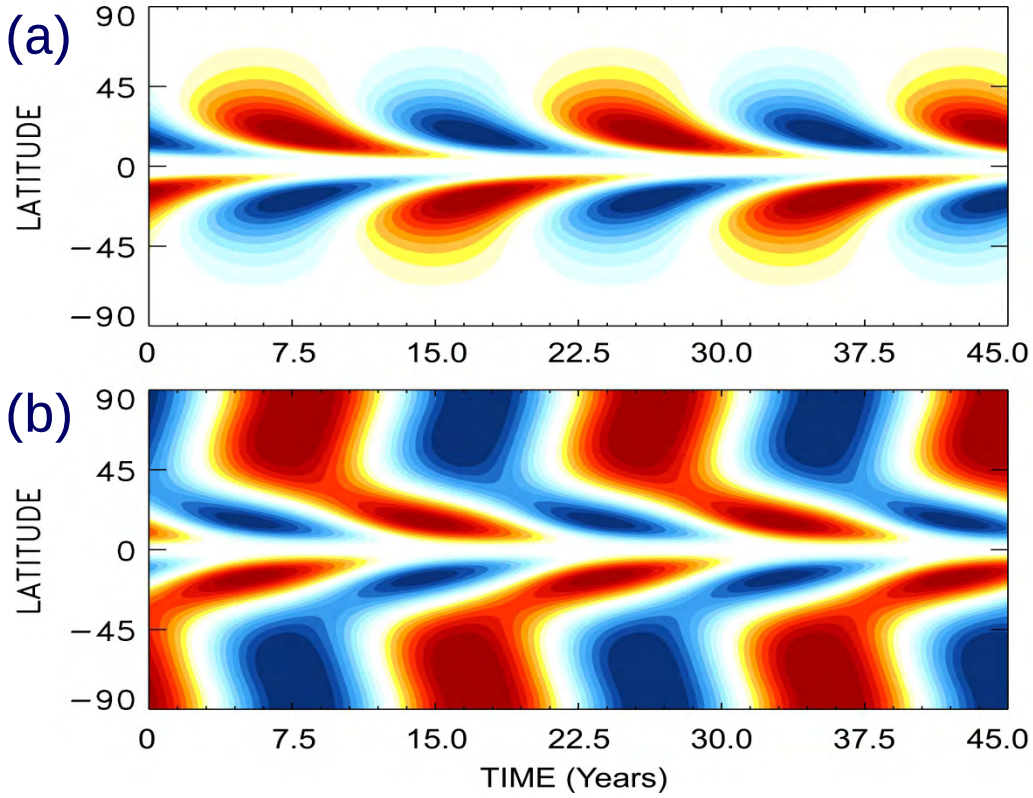

Figure: Butterfly diagram of sunspots (a) and time-latitude diagram of radial surface magnetic field (b) after the solar dynamo model of Kitchatinov & Olemskoy (Solar Phys., in press).

L. Kitchatinov, Olemskoy, Solar Phys.,2011, in press.

Contact L. Kitchatinov
kit@iszf.irk.ru

Two-step acceleration of particles in solar flares.

An analytical solution to the equation of motion for charged particles in a reconnecting current layer (RCL) with a three-component magnetic field was obtained. Given the electric field attributed to magnetic reconnection in solar flares, this solution can describe the acceleration of solar particles to high energies observed in the PAMELA space experiment. *(Oreshina A.V. and Somov B.V. , 2009, Astron. Lett. 35, 195.)*

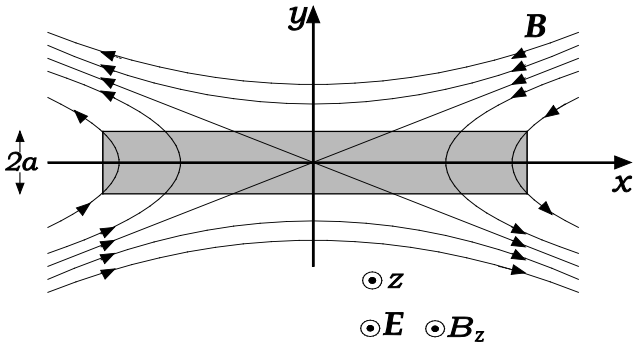

Reconnecting current layer.

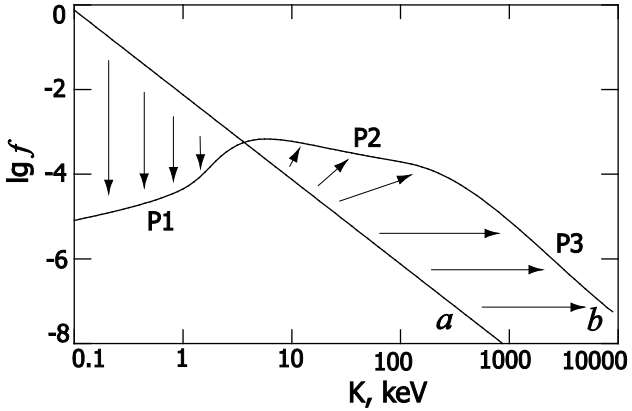

Change in the power-law distribution of particles in a collapsing trap: a – initial distribution and b – final distribution.

The problem of particle acceleration in collapsing magnetic trap in the solar corona has been solved by taking into account the Coulomb collisions. The electron spectrum at energies above 10 keV is shown to be a double-power-law one. Such spectra were observed by the RHESSI satellite in some solar flares.
(Bogachev S.A., Somov B.V., Astron. Lett. 2009, 35, 57)

Contact B.V.Somov (somov@sai.msu.ru)

Correlation of solar flare appearance with the magnetic flux from active regions

The connection between dynamics of the magnetic flux from active regions and powerful (X-class) solar flares is investigated. The normal magnetic field component to the solar surface is obtained by solving the Laplace equation with the oblique derivative as the boundary conditions obtained from SOHO MDI data. Analysis of big active regions shows that powerful flares appear after magnetic field flux increasing up to ~1022 Mx. The figure shows North and South magnetic fluxes of AR 10365 active region that traveling in solar disk produces four X-class flares. There are no characteristic magnetic field changes during a flare. This fact is in the agreement with the electrodynamical solar flare model based on current sheet decay in the corona.

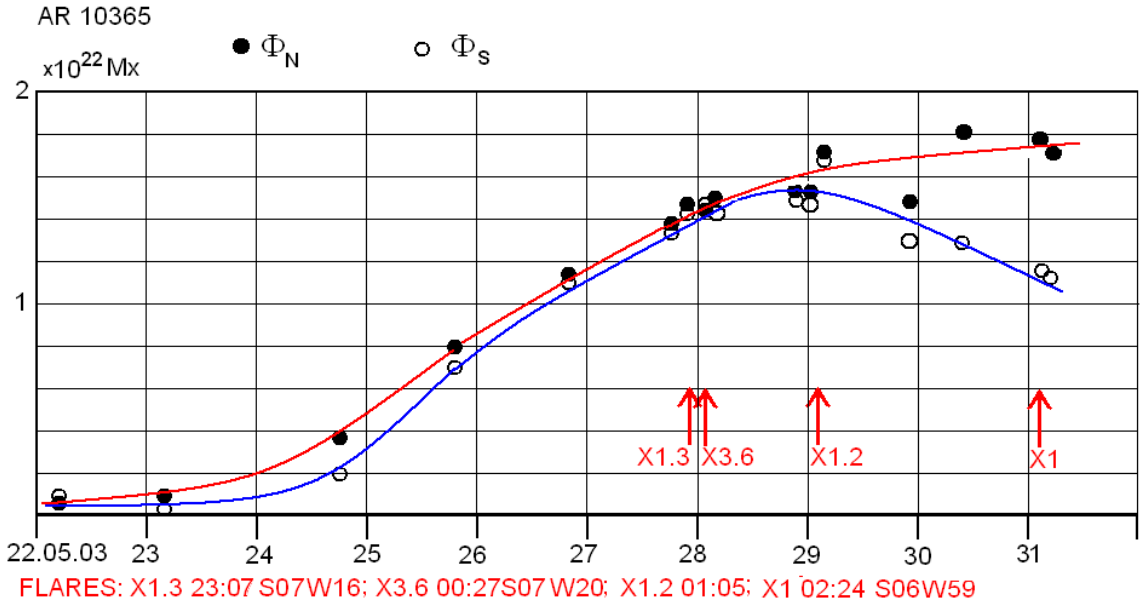

*A. I. Podgorny, I. M. Podgorny. Magnetic flux in an active solar region and Its correlation with flares. Astron. Reports., **55**. No. 7. 629–636 (2011).*

Contact I.M. Podgorny
(podgorny@inasan.ru)

Spectrum and mechanism of relativistic proton acceleration in a solar flare

Investigations based on neutron monitor data show that two components of relativistic cosmic rays are generated by a solar flare. The so called prompt component arrives from a flare with flight times and is characterized by an exponential spectrum with a parameter of $E_0 \approx 0.5$ Gev (Fig. a and b). Numerical simulations of the conditions in the flare current sheet of the Bastille flare demonstrate that charged particle acceleration up to relativistic energies takes place along a singular line in the electric Lorenz field which arises as plasma flows into a sheet. The observed exponential spectrum with $E_0 \approx 0.5$ Gev is formed during a flare and coincides with the calculated spectrum at the magnetic reconnection rate of ~107 cm s^{-1}. The reconnection rate during a flare is obtained for the first time. The delayed component which has a power law spectrum (and a relatively high isotropy, in contrast to a prompt component) is apparently formed during the diffusion of protons in plasma in the interplanetary magnetic field.

a) and b) - spectra of the prompt and delayed components of the relativistic protons for the Bastille flare. c) - the calculated spectrum.

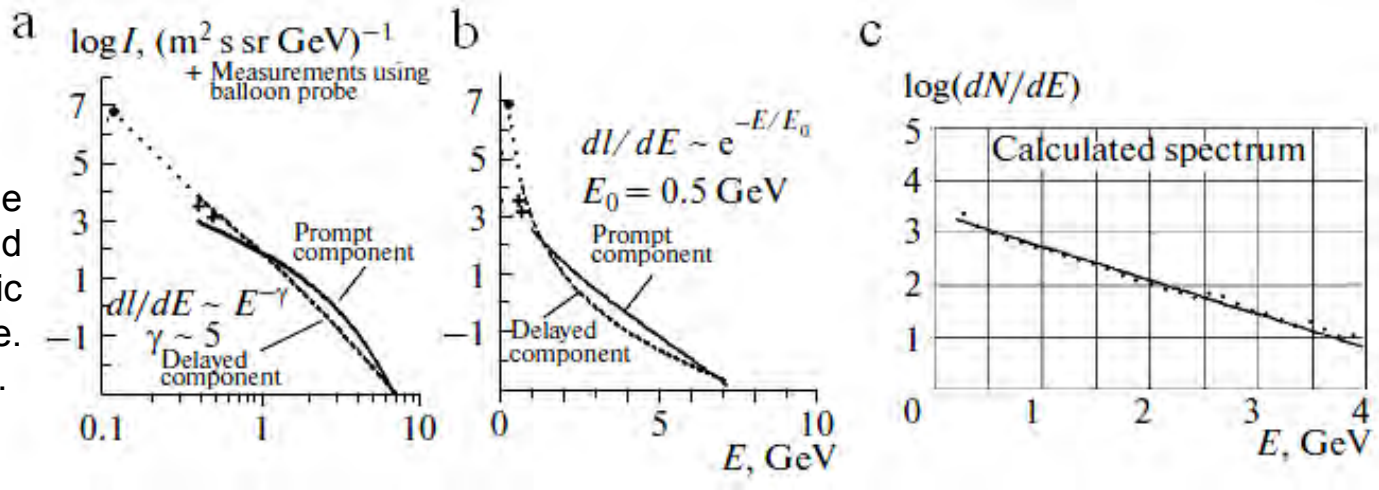

Contact I.M. Podgorny
(podgorny@inasan.ru)

*I. M. Podgorny, Yu.V. Balabin, A.I. Podgorny, E.V. Vashenyuk. Spectrum of solar flare protons // J. Atm. Solar-Ter. Phys.. **72**. № 13. P. 988–991 (2010).*

Particle acceleration and heating of solar flare plasma

For the first time **a proportionality of the plasma temperature to the logarithm of hard X-ray intensity was discovered during pre-flare and impulsive phases** of the solar flare.

The hard X-ray intensity was estimated from count rate of the anticoincidence system of the spectrometer on INTEGRAL (ACS SPI) with energy threshold of 80 keV for gamma-quanta. Moreover non-thermal processes were observed about 5 min earlier than the onset of thermal emission. These demonstrate that electrons generating hard X-ray intensity have been an initiator and main source of flare plasma heating, the particle acceleration and the plasma heating is a system with positive feed back. The proportionality disappears after beginning of plasma expansion, when plasma cooling becomes more effective than its heating by non-thermal electrons. These effects were not observed earlier due to low sensitivity of detectors (for example, NASA RHESSI).

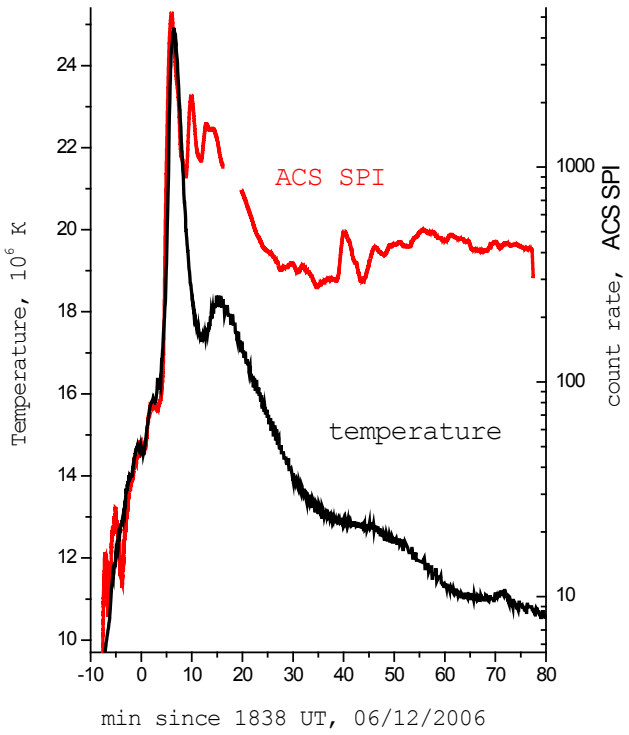

Comparing of the flare plasma temperature with the logarithm of hard X-ray intensity (>80 keV, ACS SPI) for the December 6, 2006 solar flare.

A. Struminsky and I. Zimovets, Observations of the 2006 december 6 solar flare: electron acceleration and plasma heating, Astronomy Letters, 2010, Vol. 36, No. 6, pp. 430–437.

Contact A.B. Struminsky (astrum@iki.rssi.ru)

Topological model of particle acceleration source and scenario of the event of 23 July 2002

Based on the results of complex analysis of multiwave solar data (X - and gamma radiation, optical observations, data on energetic solar protons etc.) we suggest a new topological model for the source of accelerated particles (magnetic mirror trap –"probkotron") and a new scenario of the major solar event of 23 July 2002. Solar particles (ions) may be accelerated by vortex electric field in the coronal arches of a CME up to the energies of ~10-100 MeV with a rather soft spectrum (differential spectral index ≥ 4-5). This allows to interpret some peculiar features of gamma-ray emission from the flare under consideration by taking into account nuclear collisions between accelerated and background nuclei in the Sun's atmosphere. One of the consequences of proposed model reduces to that the gamma-source of de-excitation lines (~4.1-6.7 MeV) must coincide with the region of interaction (confinement) of accelerated particles; meanwhile the source of secondary neutrons near the solar limb seems to be more effective than at the solar disk.

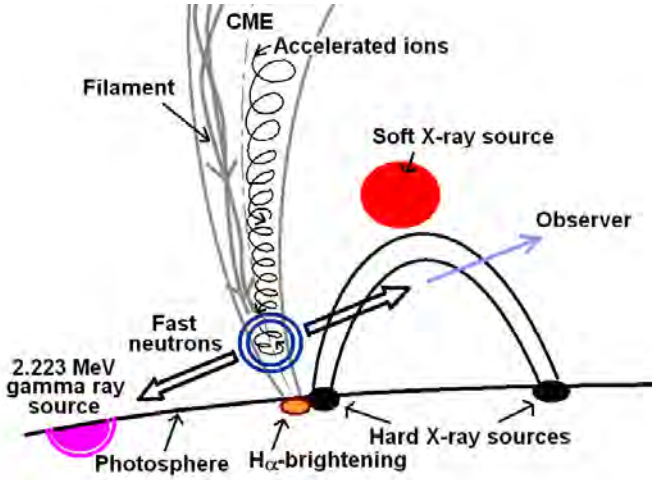

At the left – the flare of 23 July 2002. Optical data of the Big Bear Solar Observatory in the H_α-line are matched with the sources of gamma and soft X-ray emissions (*RHESSI* spacecraft) that are marked out by violet and red colors, respectively. Arrow denotes a bright chromospheric mottle of emission adjoining the sunspot umbra. At the right – a scheme for the flare source of neutral emission. Black double arrows indicating a fan-like fly away of secondary neutrons are aligned along the line of sight that links the observer, confinement region for the ions (double circle) and photospheric gamma-source of the 2.223 MeV line (double semi-circle).

G.N. Kichigin, L.I. Miroshnichenko, V.I. Sidorov, S.A. Yazev. Peculiarities of the major solar event of 23 July 2002: Source model for energetic particles. - Proc. All-Russian Conference "Solar and Solar-Terrestrial Physics-2010". SPB, Pulkovo, p.201– 204, 2010.

Contact L. Miroshnichenko (leonty@izmiran.ru)

Unified statistical distributions of solar X-ray flare durations.

The vast data base containing about 40000 X-ray solar flare events compiled and visualized as histograms and movies is collected on the site (http://dec1.sinp.msu.ru/~pavrus/) for different flare classes according to their intensities. Spacecraft measurements were analyzed during 21nd-23rd solar cycles with a time resolution of 1 min. It is found that the rising time and total duration distributions follow the lognormal laws with parameters depending on the flare class and the solar cycle. One-modal distributions cover both 'impulsive' flares (~20-30 min duration) and 'long-duration' events (> 30 min and up to many hours) at the level of 1-3 sigma.

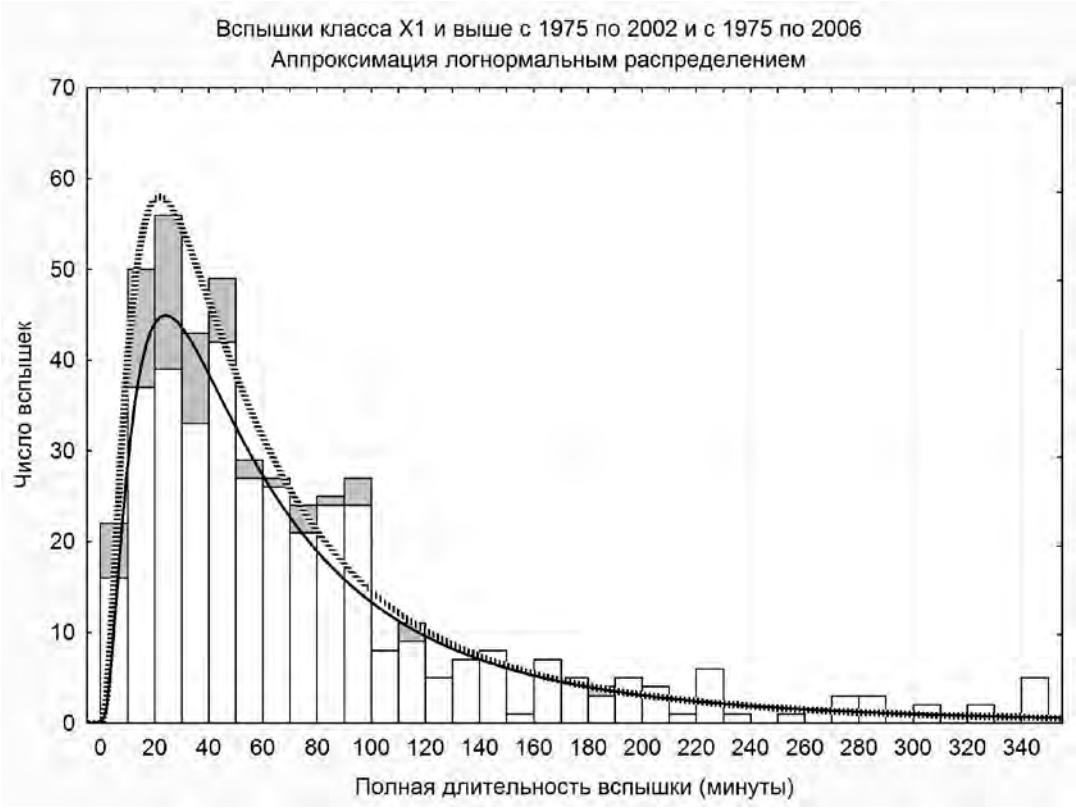

Figure shows the number of flares (ordinate) versus their total duration (min, abscissa) for the X-ray flares of the X1 class and higher, during 1975-2002 and 1975-2006 together with their lognormal approximations. Excesses and fluctuations of histograms are shown in gray.

Contact I.S. Veselovsky
(veselov@dec1.sinp.msu.ru)

Ultraviolet diagnostics of large-scale solar eruptions as a source of intensive disturbances of the space weather

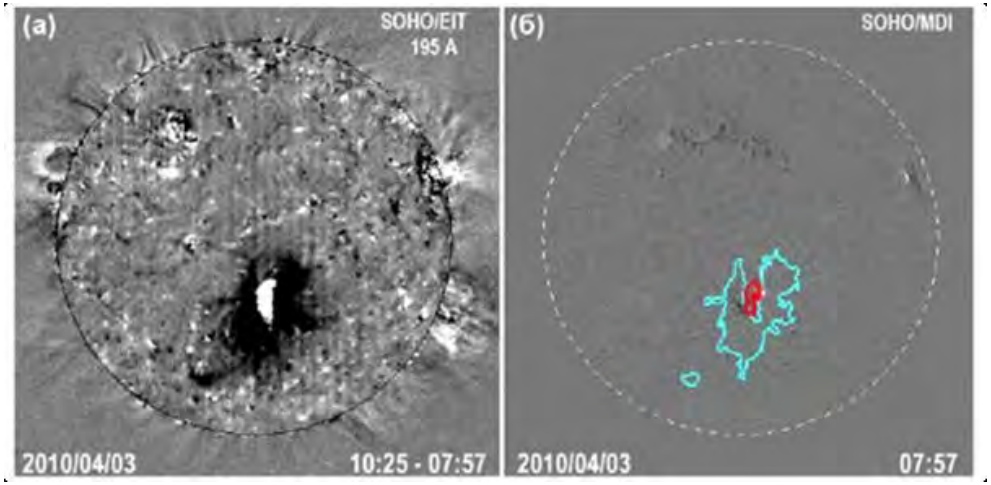

The eruption of 3 April 2010: (a) A difference image of the solar disk in the 195 A channel displaying dimmings (dark areas) and PE arcade (bright feature): (b) The contours of the dimmings and arcade against an MDI magnetogram.

The basic principles of diagnostics of solar eruptions as a source of non-recurrent space weather disturbances have been developed. The method allows early prediction of the disturbance onset time, the intensity of geomagnetic storms, and the level of cosmic ray decreases using quantitative data on the temporary depressions of radiation (dimmings) and post-eruption arcades in the ultraviolet wavelength range caused by coronal mass ejections (CME).

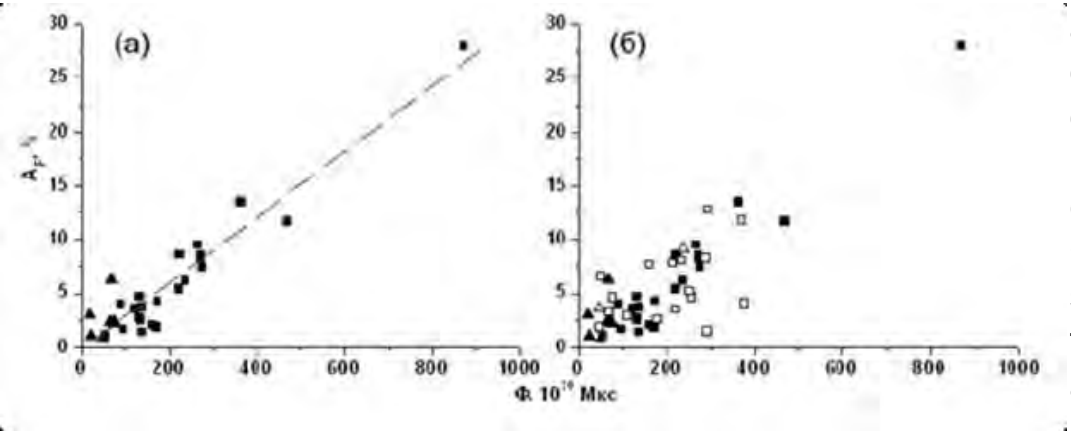

The Forbush-decrease (*AF*) as a function of the total magnetic flux from the dimmings and arcades at the photospheric level (Φ). (a) Isolated events reliably identified with a particular solar eruption (filled symbols ■ and ▲). The dashed line is the regression line. (b) All events, including the complex ones, associated with several CMEs/IMEs or presumably attributed to a solar source (open symbols □ and Δ). The squares and triangles denote, respectively, the eruptions inside and outside the active regions.

Contact I.M.Chertok (ichertok@izmiran.ru)

I.M.Chertok, A.V.Belov, V.V.Grechnev. Forbush-decrease as a function of the solar eruption parameters. http://cr2010.sinp.msu.ru/cr2010/mod/mod_07.pdf.).

Quasi-periodic fluctuations detected in MARS-EXPRESS coronal radio sounding observations.

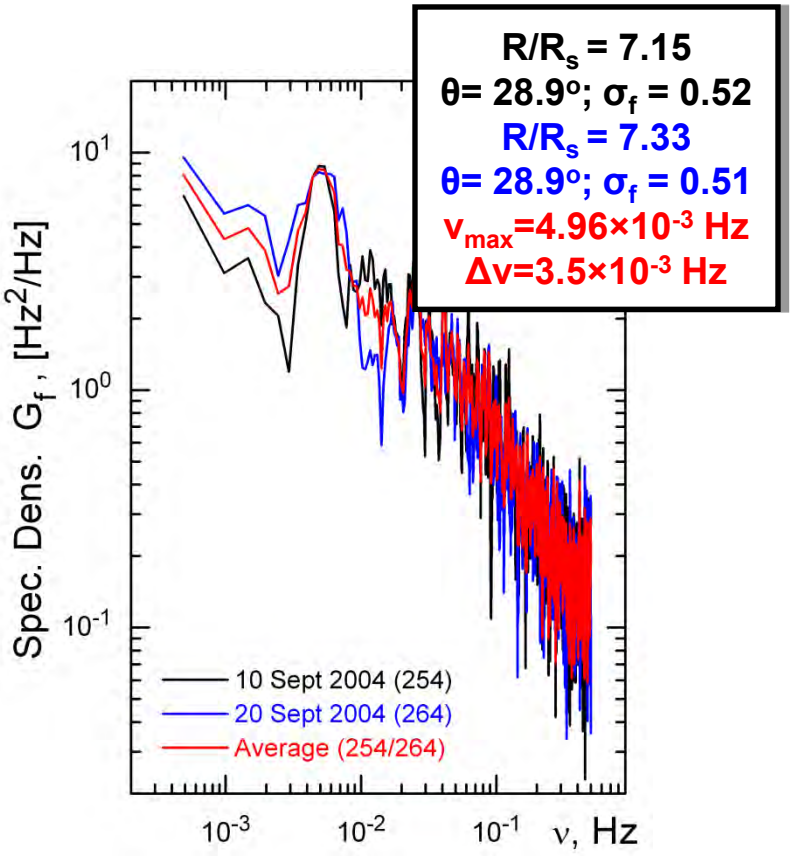

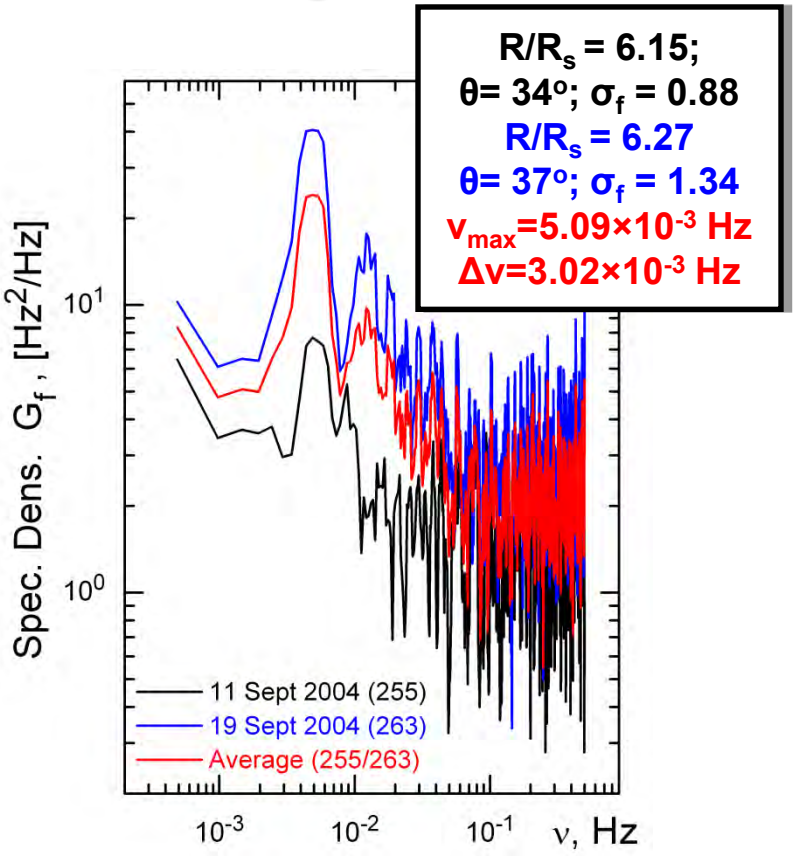

The MARS EXPRESS Coronal-Sounding Experiment has provided observational evidence of quasi-periodic frequency fluctuations of radio signals in the range 5-10 solar radii, implying that MHD (Alfven) waves with periods near 4 minutes ($\nu \approx 4$ mHz) are continuously present in the solar wind acceleration region.

The coronal-sounding observations support the idea that 5-min oscillations play an important role in the dynamics of the solar corona and solar wind.

Contact I.V. Chashey (chashey@prao.ru)

Investigation of coronal mass ejections.

The following new results are received

1. It is shown, that there is a disturbed region expanded along the CME propagation direction in front of a coronal mass ejection whose velocity u is lower than the critical u_C relative to the surrounding coronal plasma. The time difference brightness (plasma density) in the disturbed region smoothly decreases to larger distances in front of CME (A). A shock wave forms at u higher than u_C in the front part of the disturbed region manifested as a discontinuity in radial distributions of the difference brightness (shock) (B).
2. Shock wave formation ahead of a CME in a region located in the direction of the CME propagation occurs when the CME velocity relative to the solar wind exceeds the local Alfven velocity V_A. It means $u_C \approx V_A$. The formation can occur at different distances from the Sun depending on CME velocity (A).
3. At distances smaller then six solar radii the width of the shock front is of the order of the proton free path and the energy dissipation mechanism in the front appears to be collisional (B)
4. At distances more then ten solar radii in the anterior part of the collisional front a new discontinuity of much smaller width is observed to form (B).
5. Comparing the experimental dependence of the Alfven Mach number M_A on the shock wave strength ρ_2/ρ_1 with calculations within the framework of the ideal MHD substantiate the assumption that the discontinuity is a collisionless shock wave.

A

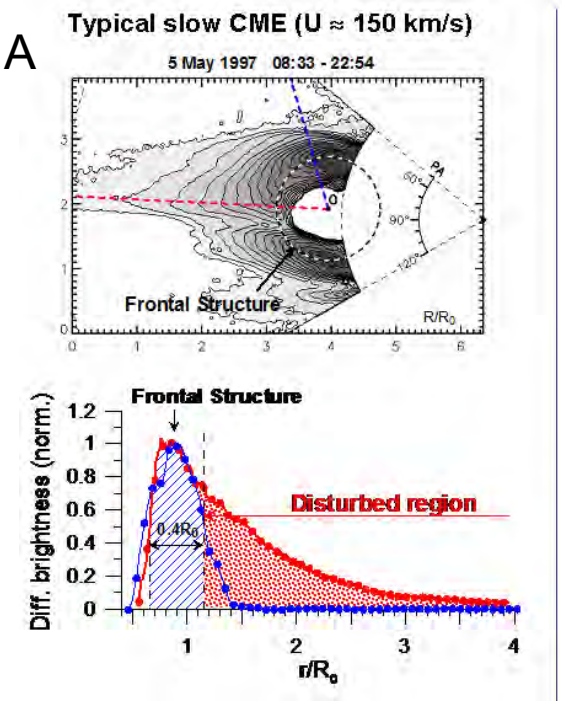

B

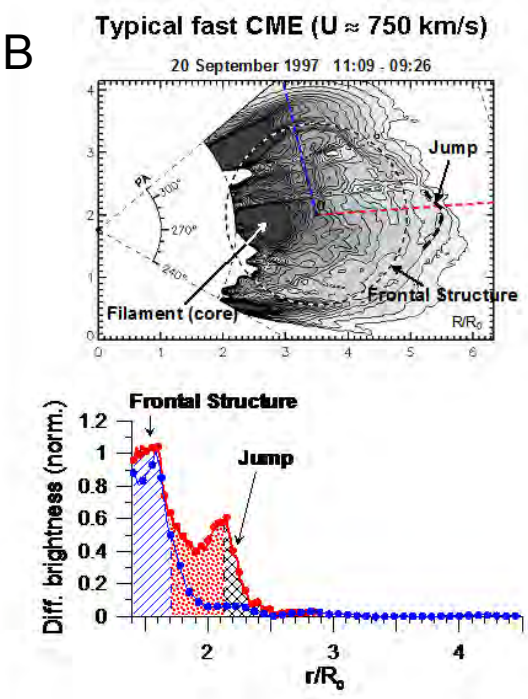

V. Eselevich, Astronomy Report, 54, 2, 197, 2010.
M. Eselevich and V. Eselevich,. Astron.Rep.55, N4, 359, 2011.

A) Difference brightness is extended along the CME propagation direction. Difference brightness section decreases smoothly with distance.

B) The shape of the difference brightness is nearly circular. A jump on a scale ≈ $0.25R_S$ is observed in the anterior of the section.

V. Eselevich (esel@iszf.irk.ru)

A forecast of solar activity variation in the 24th solar cycle.

A forecast of mean and maximum numbers of sunspot groups over the upcoming 24th solar cycle, was made using paleoastrophysical information about the solar activity throughout the last 10000 years. It was shown that from the point of view of solar paleoastrophysics the current cycle should be moderate – the maximum number of sunspot groups might reach 68-101, and the cycle average value – 34-51. Probability of a high maximum sunspot number (more than 160) predicted by some authors, was found to be weak – less than 2 %.

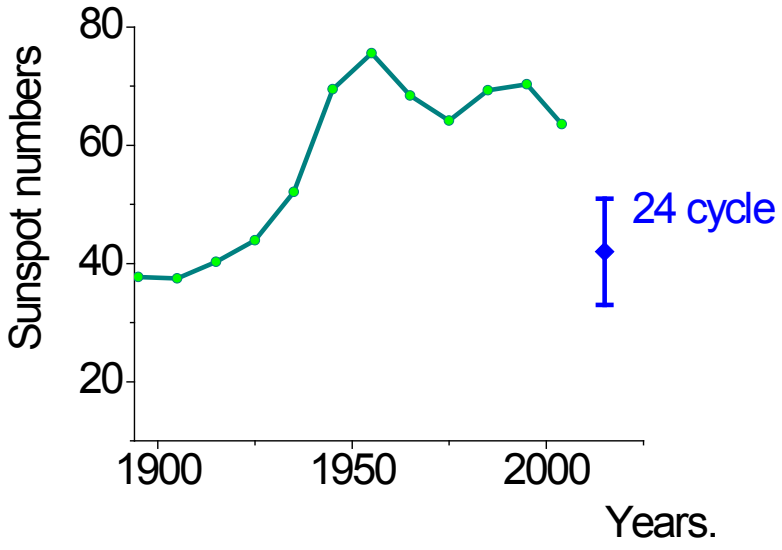

Sunspot number over the last 100 years and paleoastrophysical forecast for the current 24-th cycle.

Contact V.A. Dergachev
(v.dergachev@mail.ioffe.ru)

2. THE EARTH'S MAGNETOSPHERE

Plasma-magnetic experiment "PLASMA-F“ onboard the "SPECTR-R" spacecraft

project "RADIOASTRON"

http://www.iki.rssi.ru/plasma-f/index_e.htm

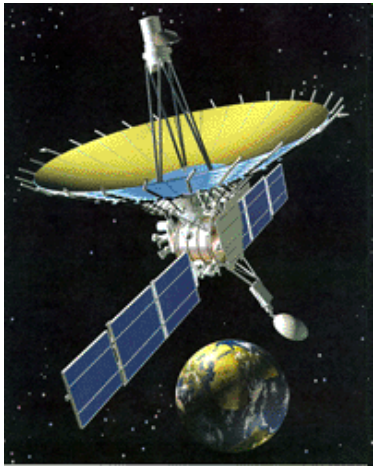

The “Spectr-R” spacecraft was successfully launched on July 18 at 6.31 a.m. (Moscow time) and was inserted into the elliptic orbit.

Project Goal – direct satellite measurements of plasma and magnetic field in the interplanetary medium and the Earth’s magnetosphere.

The "SPECTR-R" spacecraft's orbit will provide a unique opportunity to measure plasma parameters both inside as well as beyond the Earth’s magnetosphere. There were no such experiments in Russia since 2000 after the Interball-1 spacecraft finished its work. The orbital parameters are as following: the period 8.2 days, apogee – about 333 570 kilometers, perigee – 576 kilometers.

By now all instruments of Plasma-F complex are operating.

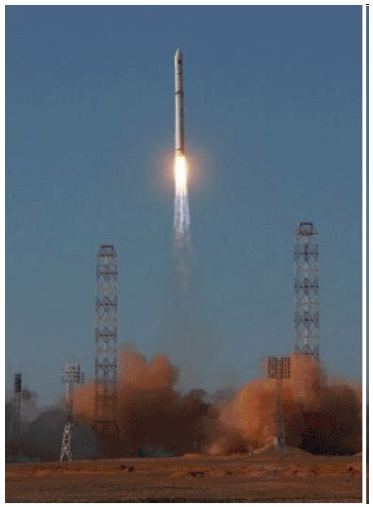

"PLASMA-F" Experiment: Main Scientific Tasks:

to monitor interplanetary medium for the purpose of space weather studies and forecasts;

to study solar wind turbulence;

to study energetic particles acceleration processes.

Principal investigator of the plasma-magnetic experiment "PLASMA-F" is **Lev Zelenyi, academician of the RAS**, director of Space Research Institute of the RAS (IKI).

Contact L.M. Zelenyi (lzelenyi@iki.rssi.ru)

Missions under development

Resonance

http://www.iki.rssi.ru/eng/index.htm

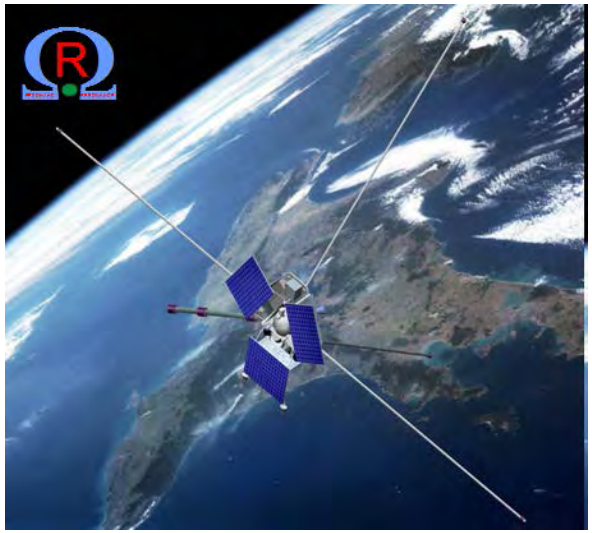

The Resonance project is aimed on the exploration of wave and particle interaction in the inner magnetosphere of the Earth.

Main scientific tasks of the project are studies of:

- dynamical characteristics of magnetospheric cyclotron maser,
- processes of plasmasphere refilling after geomagnetic disturbances,
- ring current dynamics,
- role of small-scale processes in global dynamics of magnetospheric plasma,
- processes in auroral region.

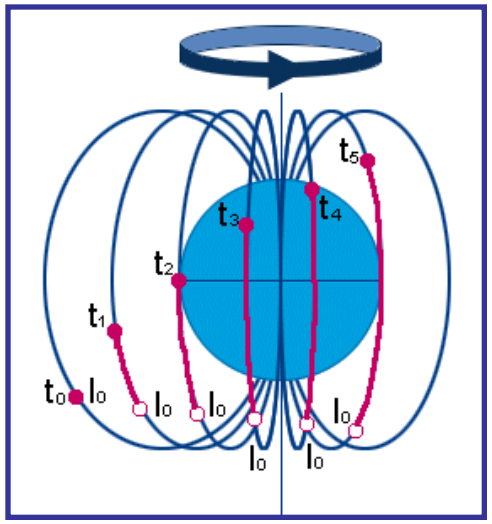

Precipitating particles
($\theta < \theta c$)

Trapped particles
($\theta > \theta c$)

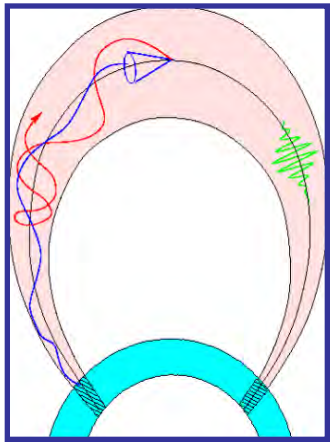

Contact M.M. Mogilevsky
(mogilevsky@romance.iki.rssi.ru)

The Earth's magnetopause and bow shock modeling using Prognoz/Interball observations

- 331 magnetopause and 232 bow shock crossings by Prognoz, Prognoz 2-6, 9 since 1972 to 1983
- 2625 magnetopause and 1150 bow shock crossings by Interball 1 during 1995 and 1999

$$y(x) = \frac{D}{\pi}\arctan\left(\frac{\pi}{D}\sqrt{2R_0(r_0 - x)}\right)$$

(r_0 – subsolar distance, R_0 – nose radius of curvature, b – bluntness of the magnetopause)

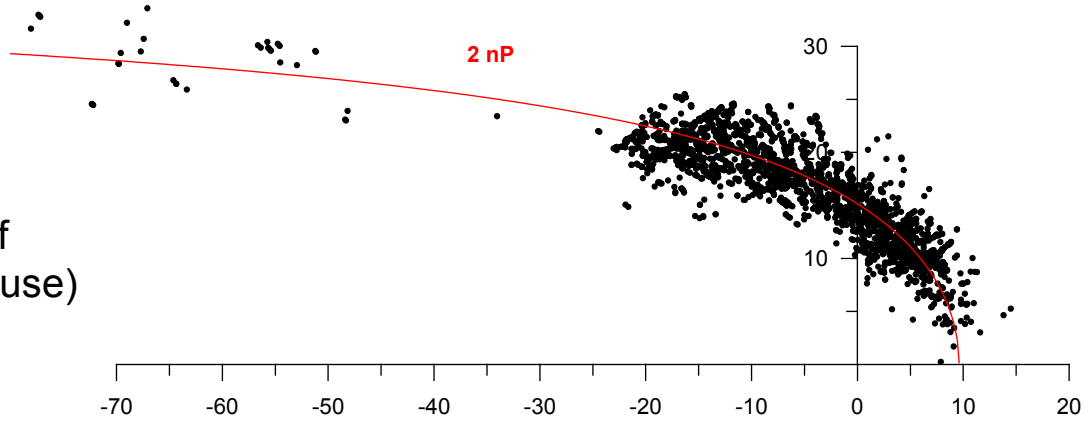

Prognoz; Prognoz 2,4,5,6,9

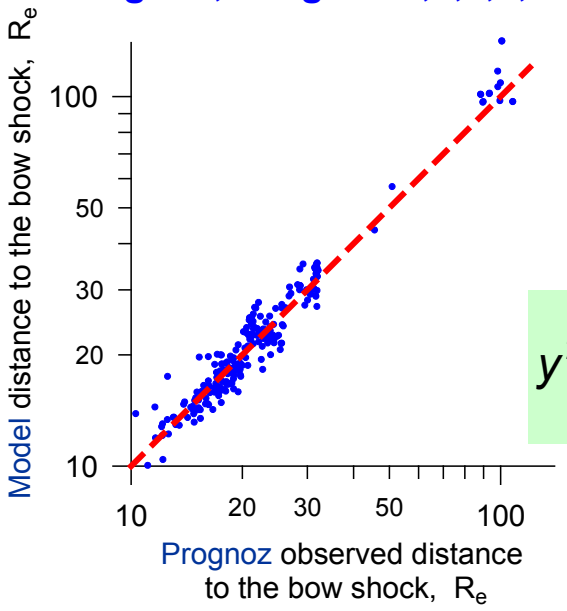

Fitted parameters - magnetopause stand off distance r_0, nose curvature radius R_0 and bluntness b = $-8\pi/3\cdot(\pi R0/D)^2$ - from MP model were used as entry parameters for the bow shock model

$$y^2(x) = 2R_s(r_0 + \Delta - x) + \frac{(r_0 + \Delta - x)^2}{M_s^2 - 1}\left(1 + \frac{b_s M_s^2 - 1}{1 + d_s(r_0 + \Delta - x)/R_s}\right)$$

M.I.Verigin et al., Geomagnetism and Aeronomy, 2009, Vol. 49, No. 8, pp. 1176–1181.

Contact M.I.Verigin (verigin@iki.rssi.ru)

Investigation of the hot flow anomaly structure at the Earth's bow shock

The structure of the Hot Flow Anomaly (HFA) detected by Interball-Tail 96/03/14 near the Earth's bow shock was investigated. The work is based on data acquired by ion spectrometer SKA-1, electron spectrometer ELECTRON, and magnetometer MIF-3. The orientation of interplanetary current sheet that caused formation of HFA was found. Several characteristic regions within the HFA were identified from dynamic spectra of electrons and ions. Using the geometry of the bow shock it was shown, that electric field on both sides of the current sheet is directed towards this sheet. This corresponds to previous ideas on the reason of HFA's formation.

The velocity of the HFA's motion along the bow shock front and transverse dimension of HFA was estimated. We found that HFA was expanding sideways from the current sheet. Detailed analysis of ion velocity distributions within HFA showed that it has complicated structure and consists of two parts. A part of HFA has sunward directed velocity indicating to convective structure of the HFA. Analysis of magnetic field and ion velocity distributions allowed to locate a source of thermal and convective energy.

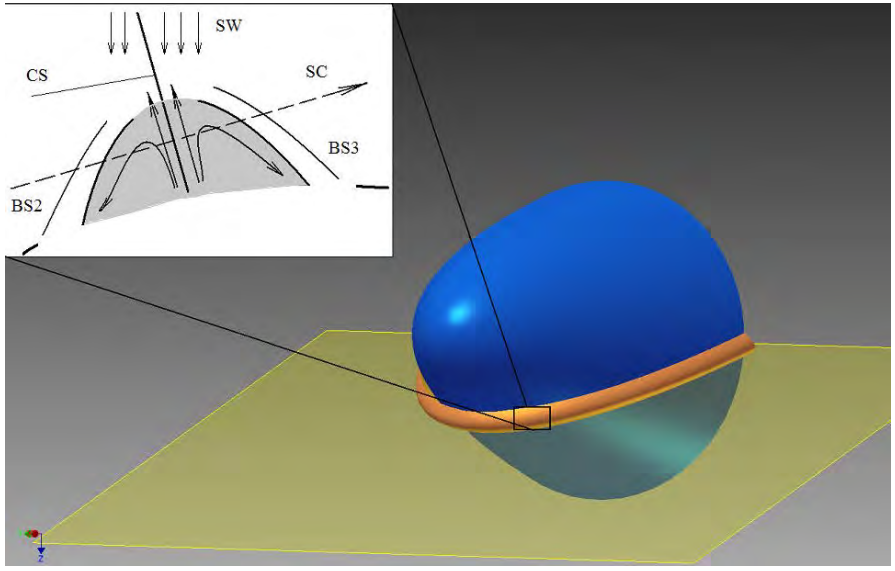

Mechanism of formation and internal structure of HFA. Blue structure shows the Earth's bow shock, yellow plane marks current sheet, orange belt - hot plasma. Upper left scheme: BS2, BS3 secondary bow shocks, formed on HFA as on an obstacle, SW – solar wind flow, CS – current sheet section, dashed line shows the spacecraft (SC) possible trajectory, grey color – hot plasma within HFA, arrows show possible convection flows.

A.Shestakov, O. Vaisberg, Geomagnetizm and Aeronomie, accepted.

Contact A. Shestakov
sartiom1@yandex.ru

Plasma pressure distribution in the inner Earth's magnetosphere according to THEMIS mission data

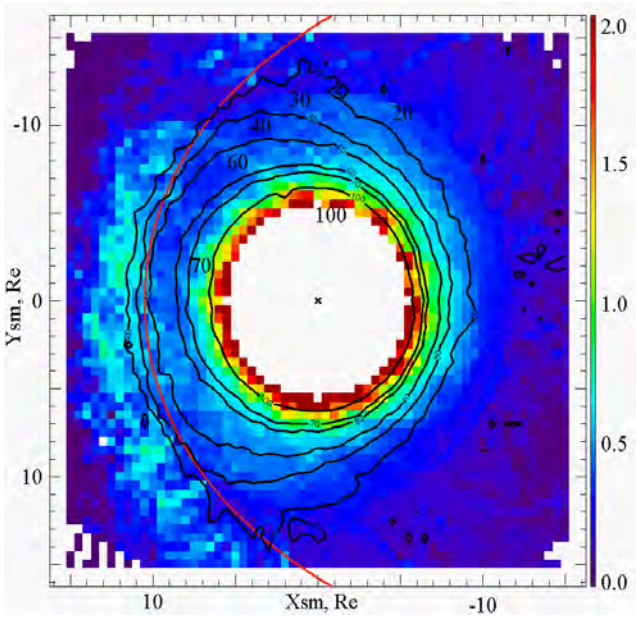

The structure of the averaged plasma pressure distribution in the plasma ring around the Earth at geocentric distances of ~6–10*RE* has been determined. The moments of ion distribution function measured on the international THEMIS mission satellites have been used. The plasma pressure distribution in the equatorial plane at 15*RE* > XSM > –15*RE* and 15*RE* > YSM > –15*RE* has been statistically studied. The radial dependence of the plasma pressure at the day–night and morning–evening meridians has been analyzed. It has been indicated that the plasma ring around the Earth has a structure, which is close to being azimuthally symmetric. The achieved results have been compared with the pressure distributions obtained previously. It has been indicated that in the overlapping regions, the achieved results agree with the previously obtained data within the pressure determination errors.

I. Kirpichev and E. Antonova, Plasma pressure distribution in the equatorial plane of the Earth's magnetosphere at geocentric distances of 6–10RE according to the international THEMIS mission data, Geomagnetizm and Aeronomie, 51(4), 450-455, 2011.

Contact I.Kirpichev
ikir@iki.rssi.ru

Particle acceleration in the magnetotail current sheet (1).

On the basis of analysis of more than 400 crossings of Plasma Sheet Boundary Layer (PSBL) by Cluster spacecraft (s/c) (in 2001-2004) and of about 1000 PSBL crossings by Geotail s/c (1993-1995) it was revealed for the first time that **there are two kinds of accelerated ion beams** which are observed in PSBL in different periods of geomagnetic activity.

During geomagnetically quiet periods energy-collimated ($\Delta V_{||}/V_{||}$ ~ 0.1) **field-aligned ion beams (beamlets)** are usually observed in PSBL. Beamlets have the size along magnetic field direction of the order of tens Earth radiuses (R_E) and are strictly localized in the direction perpendicular to the magnetic field (< 1 R_E). The duration of ion beamlets may exceed 20 min. Beamlets are accelerated due to ion resonant interaction with the Current Sheet (CS) in spatially localized sources (resonances) in the distant magnetotail (> 110 R_E from the Earth) but in the region of closed magnetic field lines. Ion beamlet acceleration is quasi-steady and is due to potential dawn-dusk electric field, it is not related with magnetic reconnection process (Figure, left part).

During disturbed geomagnetic periods ion beams are characterized by large energies (up to 200 keV) and parallel temperatures (the width of ion velocity distribution functions $\Delta V_{||}/V_{||}$ > 0.4). These ion beams are accelerated in the CS closer to the Earth (< 50 R_E) and their acceleration sources are located near the magnetic X-line (Figure, right part) that is confirmed by the anisotropic electron velocity distribution functions registered simultaneously near the lobeward edge of ion beams. Inductive electric fields play an important role in ion acceleration.

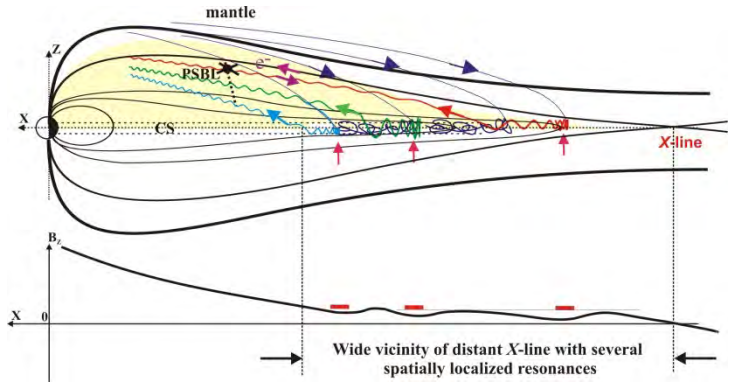

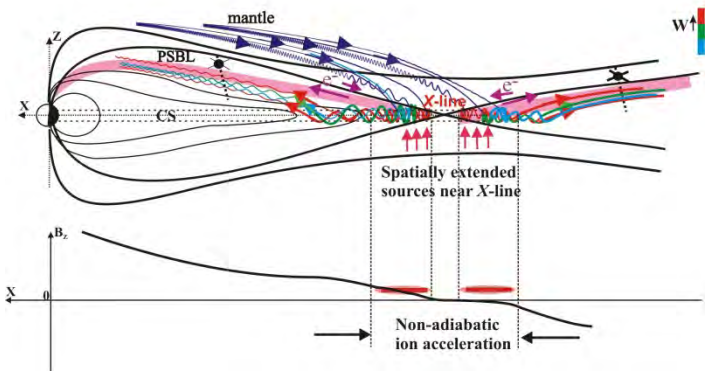

Grigorenko E.E., L.M. Zelenyi, M.S. Dolgonosov, J.-A. Sauvaud, Spatial and temporal structures in the vicinity of the Earth's tail magnetic separatrix. Cluster observations, Book of Proceedings of 15th Cluster Workshop and CAA School, 435-453, 2010.

Contact E.E. Grigorenko
elenagrigorenko2003@yahoo.com)

Particle acceleration in the magnetotail current sheet (2).

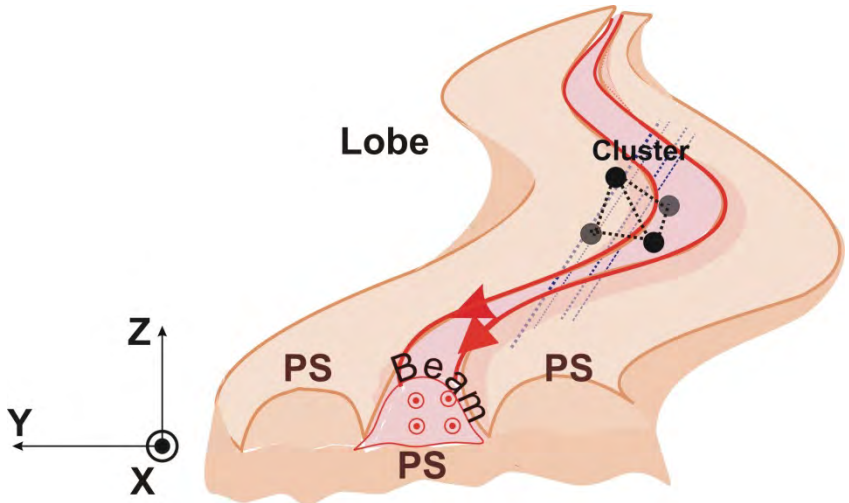

An illustration of high-latitude PSBL surface consisting of magnetic flux tubes of finite cross-section and containing either ion beams (shown by the pink color) or almost isotropic Plasma Sheet-like plasma (shown by light-brown color).

Multipoint measurements provided by Cluster s/c in the Earth's magnetotail allow revealing that during quiet or moderately disturbed geomagnetic periods the lobeward surface of the PSBL is not uniform in dawn-dusk direction and consists of magnetic flux tubes which are either connected with the localized ion acceleration sources in the CS and so contain accelerated ion beams or disconnected with acceleration sources and so are filed by more isotropic Plasma Sheet-like plasma (see the Figure). The characteristic size of magnetic flux tubes in the direction perpendicular to the main magnetic field does not exceed 1 R_E.
It was also shown that large-scale (f ~ 0.004 – 0.02 Hz) Alfven fluctuations are usually observed in the PSBL during the periods of high-velocity ion beam propagation (when ion field-aligned velocity exceeds double value of local Alfven velocity). The Kelvin-Helmholtz instability, arising in the boundary between high-velocity plasma flow and almost motionless surrounding plasma is a possible source for such large-scale perturbations.

Grigorenko, E. E., Burinskaya, T. M., Shevelev, M., Sauvaud, J.-A., and Zelenyi, L. M. Large-scale fluctuations of PSBL magnetic flux tubes induced by the field-aligned motion of highly accelerated ions, Annales. Geophysicae, 28,1273-1288, 2010.

Contact E.E. Grigorenko
(elenagrigorenko2003@yahoo.com)

Thin Current Sheets in Collisionless Plasma: Equilibrium Structure, Plasma Instabilities, and Particle Acceleration

Thin current sheets have been discovered and investigated by spacecraft observations in the Earth's magnetotail in the last decades. Their formation is attributed to dynamic processes occurring in a collisionless space plasma during geomagnetic perturbations and near the magnetic reconnection regions. The models that describe thin current structures in the Earth's magnetotail are based on the assumption of the quasi-adiabatic ion dynamics in a relatively weak magnetic field of the magnetotail neutral sheet, where the ions can become unmagnetized. It is shown that the ion distribution can be represented as a function of integrals of particle motion---the total energy and quasi-adiabatic invariant. Theoretical results are compared with the observational data from the Cluster spacecraft. Various plasma instabilities developing in thin current sheets are investigated. The evolution of the tearing mode is analyzed, and the parameter region in which the mode can grow are determined, the paradox of complete stabilization of the tearing mode in current sheets with a nonzero normal magnetic field component is thereby resolved. Over a wide range of current sheet parameters and propagation directions of large-scale unstable waves, various modified drift instabilities - kink and sausage modes - can develop. Based on the concept of a turbulent electromagnetic field excited as a result of the development and saturation of unstable waves, a mechanism for charged particle acceleration in turbulent current sheets is proposed and the energy spectra of the accelerated particles are obtained.

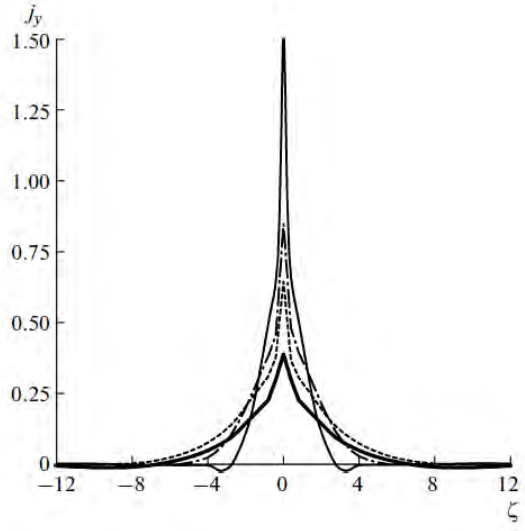

Artemyev A. V., A. A. Petrukovich, R. Nakamura, and L. M. Zelenyi, J. Geophys. Res., 115, A12255, doi:10.1029/2010JA015702, 2010.
Petrukovich, A. A., A. V. Artemyev, H. V. Malova, V. Y. Popov, R. Nakamura, and L. M. Zelenyi , J. Geophys. Res., 116, A00I25, doi:10.1029/2010JA015749 , 2011.

Contact L. Zelenyi, A. Petrukovich, A. Artemyev (ante0226@yandex.ru)

Origins of plasma sheet B_y

With 11 years of Geotail measurements we analyzed sources of plasma sheet B_y and constructed a model, depending on IMF B_y, coordinates X, Y, and geodipole tilt angle. B_y dependence on dipole tilt due to the neutral sheet warping and hinging has an odd (antisymmetric) profile with respect to Y. In addition, a new, even with respect to Y, B_y component was discovered, which is positively correlated with dipole tilt with the maximal amplitude $\pm$1–2 nT. In the postmidnight sector the dipole tilt effects in B_y almost cancel each other, while at the premidnight sector they are summed up and are comparable with the IMF penetration. Such season-dependent net B_y creates a principal azimuthal asymmetry of the magnetotail and is consistent with some polar convection and aurora observations. Plasma sheet B_y is often substantially larger than the statistically expected value. This effect can be understood as “amplification” due to internal plasma sheet dynamics. As a result an asymmetric tail of the B_y distribution forms, causing certain overestimation of the regression coefficients in statistical models.

Petrukovich, A. A. (2011), Origins of plasma sheet By, J. Geophys. Res., 116, A07217, doi:10.1029/2010JA016386

Contact A.A. Petrukovich
(apetruko@iki.rssi.ru)

Ion cooling in the plasmasphere during magnetic storm initial phase

INTERBALL 2 and MAGION 5 measurements in the Earth's inner magnetosphere revealed that during magnetic storm main phase plasmaspheric ion temperature mostly fell down while ion density either increased or stayed at the level typical for undisturbed conditions.

A physical mechanism describing outward proton drift which causes ion temperature decreasing during magnetic storm is considered. Model temperatures (T_r) well agree with experimental data ($T_{r,obs}$).

It is shown that for the thermal plasma in the equatorial plane the third adiabatic invariant is conserved even in the processes with characteristic time less than charged particle drift time around the Earth.

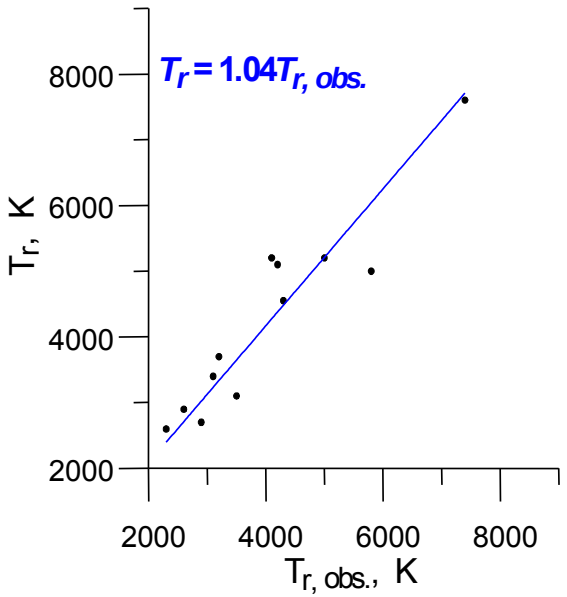

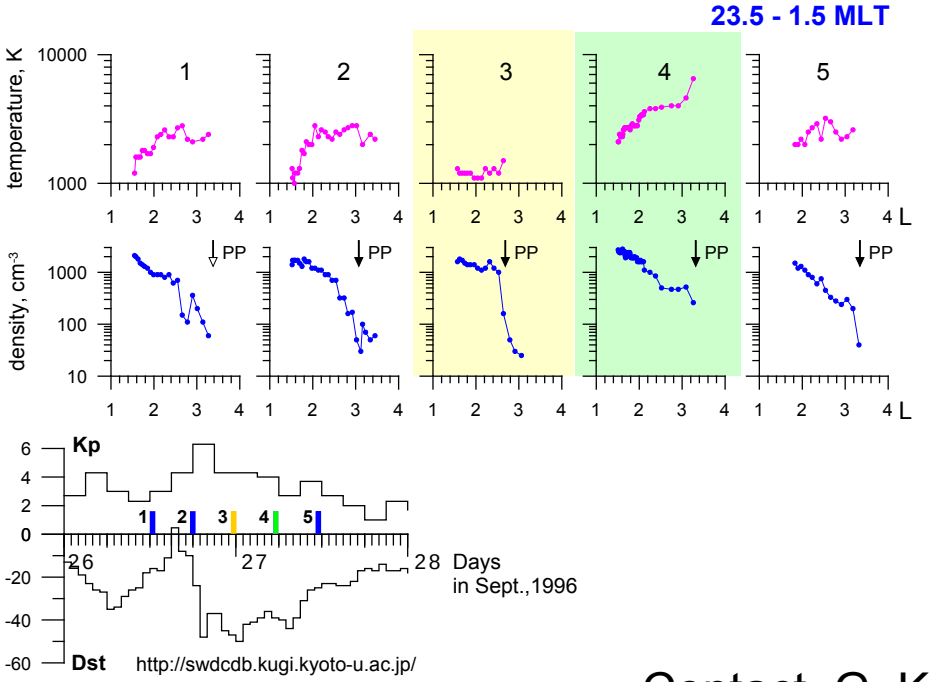

M. I. Verigina, G. A. Kotovaa, V. V. Bezrukikha, V. V. Bogdanovb, and A. V. Kaisin, Geomagnetism and Aeronomy, 2011, Vol. 51, No. 1, pp. 39–48.

Contact G. Kotova (kotova@iki.rssi.ru)

Experimental evidence for direct penetration of ULF waves to the magnetosphere from the solar wind and their possible effect on acceleration of radiation belt electrons

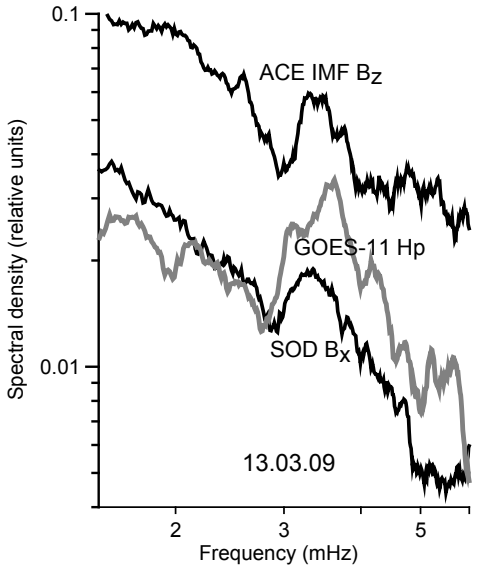

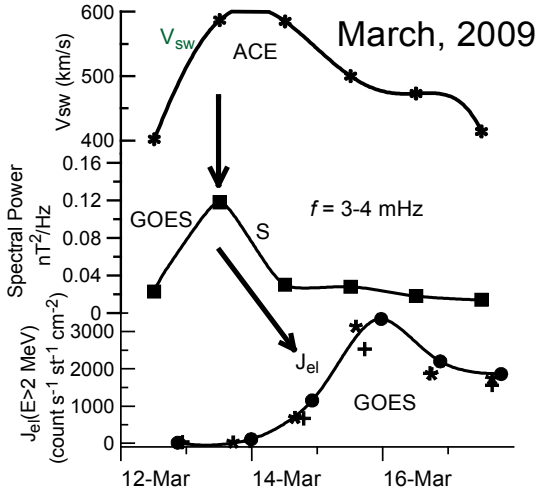

Event of March 12–19, 2009, when the high-speed stream of the solar wind, carrying the ULF waves of mHz range passed the Earth's magnetosphere, was analyzed. The stream caused a weak magnetic perturbation (Dst_{min} = –28 nT). On March 13, fluxes of energetic electrons (up to relativistic energies) began to increase in the magnetosphere. Comparison of ULF oscillations observed in the solar wind, magnetosphere and at the Earth's surface, revealed the presence of sustainable spectral peak between 3 and 4 mHz in all these regions (top figure). This suggests the direct penetration of waves from the solar wind into the magnetosphere. Next ULF oscillations gradually accelerated the seed electrons in the magnetosphere first to hundreds of keV, and then to a few MeV, providing a peak flux of relativistic electrons on the second or third day after the peak of the solar wind speed (bottom figure).

Chain of processes leading to appearance of the killer electrons: Solar wind high-speed stream -> ULF waves in the solar wind and in the magnetosphere -> relativistic electrons

Contact A.S. Potapov
(potapov@iszf.irk.ru)

Potapov, A. S. and Polyushkina T. N.: Experimental evidence for direct penetration of ULF waves from the solar wind and their possible effect on acceleration of radiation belt electrons, Geomagnetism and Aeronomy, 50(8), 28–34, 2010.

Standing slow magnetosonic waves excited in the plasmasphere by the solar terminator motion

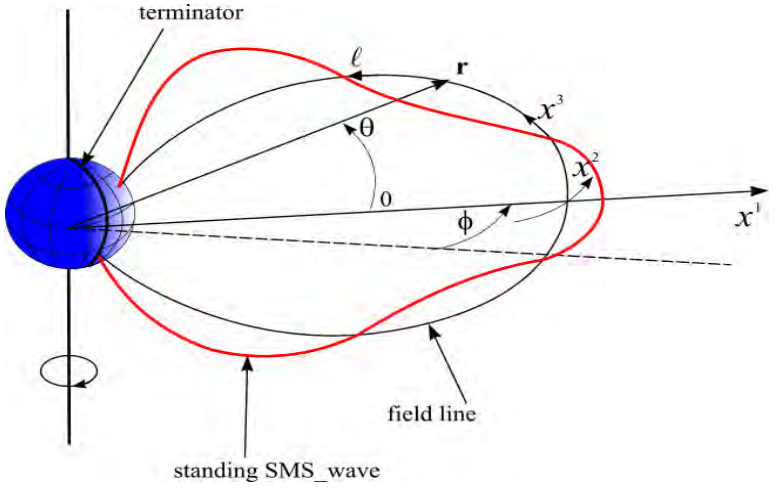

Fig.1 The standing slow magnetosonic wave excited in the plasmasphere by the solar terminator motion

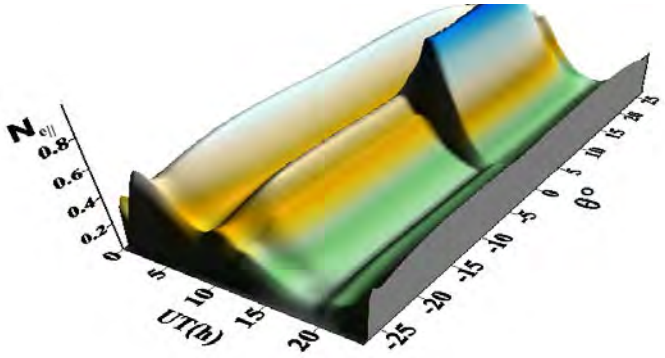

Fig.2 Theoretically calculated diurnal amplitude of the total electron content $N_{e||}$ ($10^{16}m^{-2}$), associated with SMS-wave (over Japan 14.06.2008 from the ionosphere – q=25° to the equatorial plane q=0°.

Total electronic content (TEC) oscillations were registered in GPS observations over Japan associated with the terminator motion over the magnetoconjugated region of the ionosphere. It was suggested, that these oscillations are connected with slow magnetosonic (SMS) waves in the plasmasphere (Fig.1). A problem of the structure and spectrum of SMS-waves in a dipole plasmasphere has been solved. It is shown that the oscillation of the first few harmonics of standing slow magnetosonic waves can explain the observed oscillations of total electronic content (Fig.2).

Afraimovich, E.L., Edemskiy, I.K., Leonovich, A.S., Leonovich, L.A., Voeykov, S.V., and Yasyukevich, Y.V. MHD nature of night-time MSTIDs excited by the solar terminator. Geophys. Res. Lett. 36, L15106, doi:10.1029/2009GL039803, 2009.

Leonovich A.S., Kozlov D.A., Edemskiy I.K. Standing slow magnetosonic waves in a dipole-like plasmasphere, Planet. and Space Sci., Vol. 58, 1425–1433, 2010.

Contact A.S. Leonovich
(leon@iszf.irk.ru)

ULF wave (1-6 mHz) signature of a magnetic storm

Based on the analysis of magnetic observations by the globally distributed ground-based stations, the geomagnetic pulsations in the Pc5-Pi3 range during several strong magnetic storms were considered. The ULF maps have been constructed in the coordinates (geomagnetic latitude – MLT). The typical ULF wave signature for the different storm phases has been established .

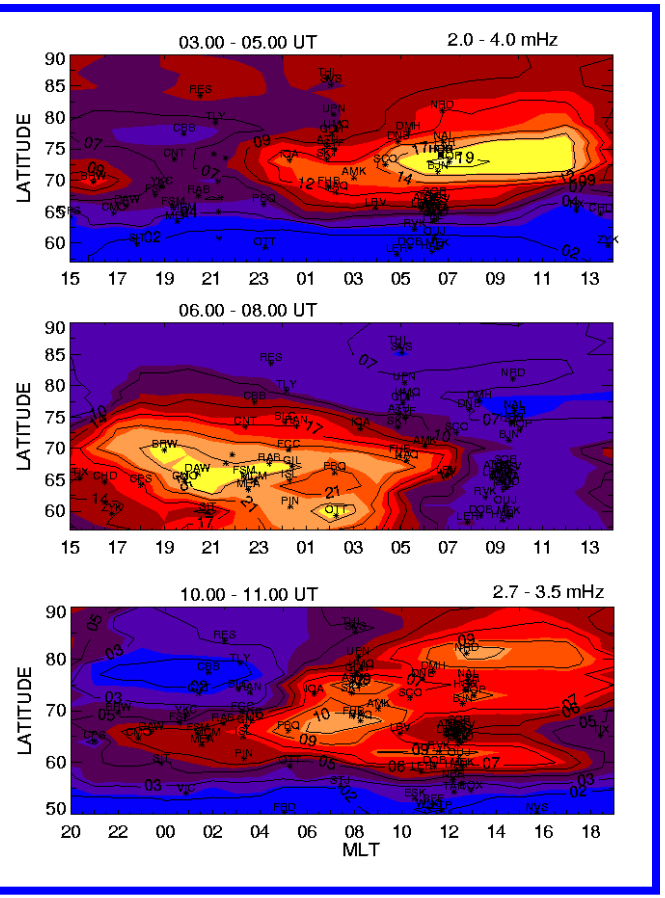

In the storm initial phase, the strongest 1-6 mHz Pc5 geomagnetic pulsations are observed in the morning sector in polar (Φ>70) latitudes.

In the storm main phase, the strongest irregular 1-6 mHz Pi3 magnetic pulsations are observed at the night side of the auroral zone, and the largest continuous Pc5 pulsations are typical for the morning side of the auroral latitudes.

In the storm recovery phase, the ULF activity shifts to the polar latitudes, and the strongest Pc5 pulsations are recorded at the Φ > 70 mostly in the day time sector.

N.G. Kleimenova (kleimen@ifz.ru)
O.V. Kozyreva (kozyreva@ifz.ru)

The new ULF-index of geomagnetic pulsation activity

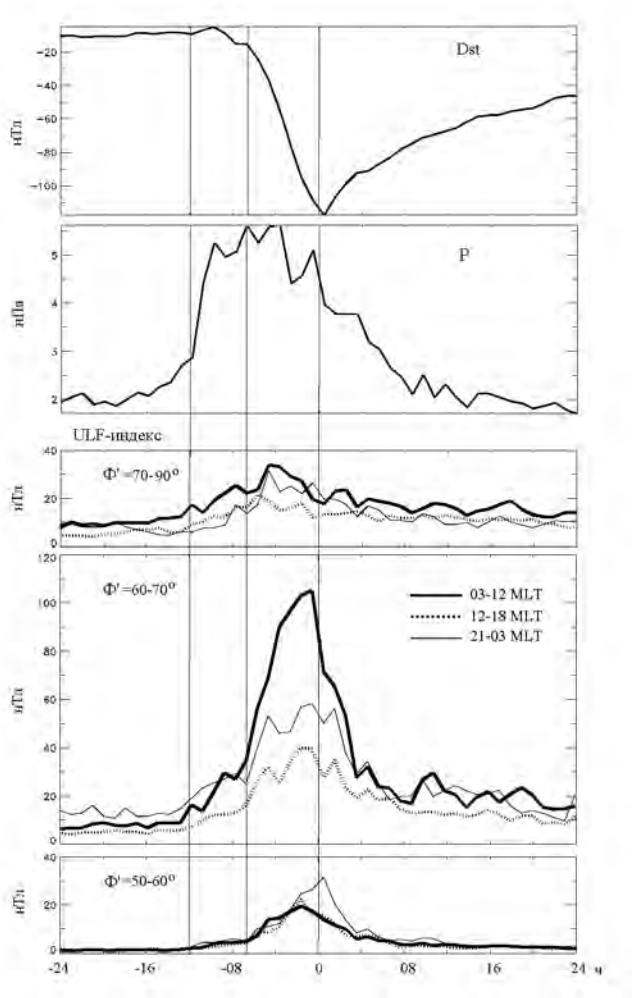

The new ULF-index of the geomagnetic Pc5 (f=1.7-6.0 mHz) pulsation activity has been developed for any given latitude range. The empirical model of the spatial-temporal Pc5 pulsation dynamics has been elaborated applying to the different phases of magnetic storms, caused by the coronal mass ejection (CME). It was found that in the initial storm phase, the strongest ULF wave activity was observed at the morning side of the polar latitudes, probably, due to direct penetration of the solar wind hydromagnetic waves. In the storm main phase, the strongest pulsation activity was not observed at the night sector, as it was commonly expected. The strongest Pc5 range wave amplitude was recorded before the local noon at the auroral zone latitudes demonstrating the typical signature of the field line resonance structure.

Contact O.V. Kozyreva
(kozyreva@ifz.ru)

Dst-index averaged for 19 strong magnetic storms, solar wind dynamic pressure (P), and ULF-index at different latitude zones for 3 intervals of local magnetic time: morning (03-12 MLT), afternoon (12-18 UT), and night-time (21-03 MLT). The vertical fine lines show the border of different storm phases.

Generation of subauroral proton emissions.

IMAGE

geomagnetic pulsations

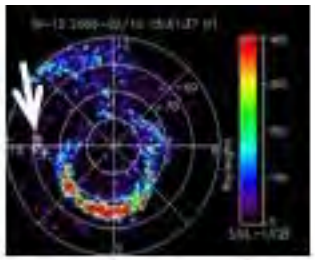

15:31 UT

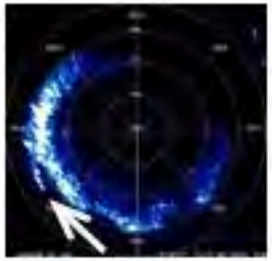

17:04 UT

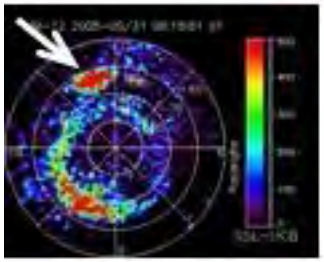

08:16 UT

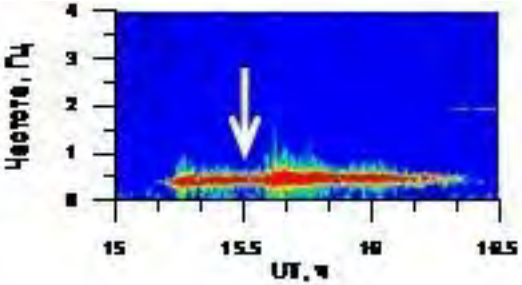

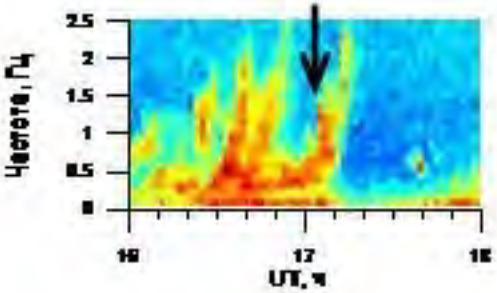

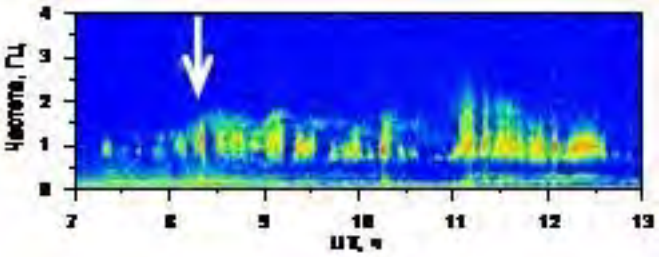

Optical measurements on IMAGE were compared with simultaneous ground-based data on geomagnetic pulsations of 0.1-5 Hz. These pulsations are the indicator of electromagnetic ion-cyclotron waves.
It is shown that energetic electron (E>10 keV) precipitations producing proton (Hα) emissions, are caused by cyclotron instability of ring current protons. Space-time features of proton emissions depends on the geometry and evolution of the contact region between cold and hot plasmas in the magnetosphere and also on the solar wind ram pressure.

Contact A.G. Yakhnin
(yahnin@pgia.ru)

Top panels – quiet conditions, proton spot.
Middle panels – substorm, proton arcs - plasmaspheric tail or plume.
Bottom panels – ram pressure impulses, proton flashes.

3. THE EARTH'S IONOSPHERE

A study of the behavior of intermediate falling sporadic layer height at mid latitdes

During prolonged magnetically quiet period for the first time the midlatitude intermediate falling sporadic layer of the ionosphere was examined in details. Intermediate falling layer forms twice a day (in the morning and in the evening) in the lower F region and continuously descends into the E-region.

It was established empirically that times of morning layer formation are grouped around local dawn times at the Earth's surface plus 1 hour, while evening layer forms at times close to dusk at the Earth's surface minus 1 hour. According to our observations the phenomenon of the intermediate falling layer has no exact 12 hour periodicity but determined by local dawn and dusk times, incongruous with well known results, obtained by incoherent scattering radar in Arecibo [Christakis et al., 2009, Ann. Geophys. 27(3), 923-931].

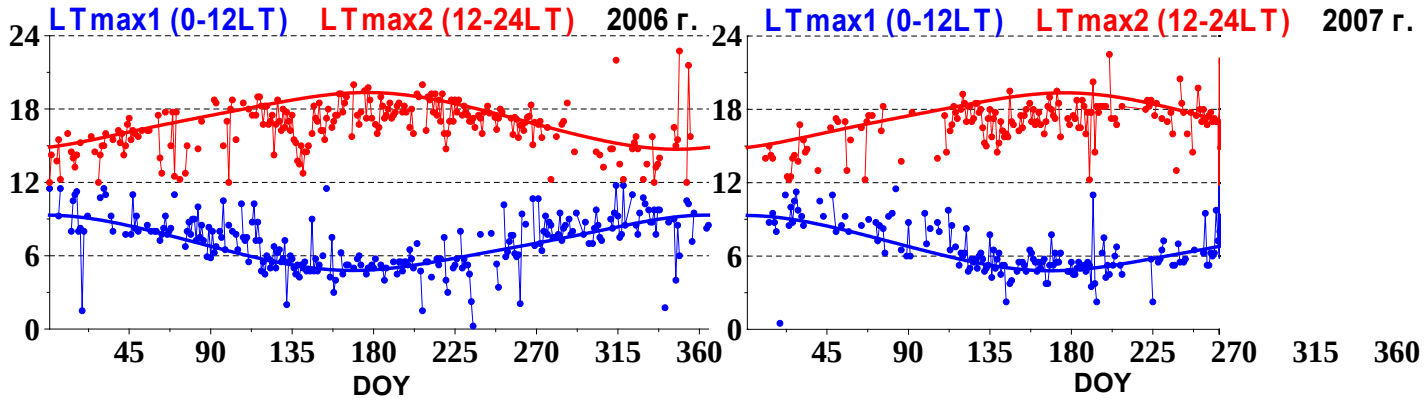

Seasonal variations of the formation times for the morning (LTmax1, blue circles) and evening ((LTmax2, red circles) falling intermediate layers. Solid lines corresponds to the local dawn time + 1 hour and local dusk time – 1 hour.

Zherebtsov G.A., Kurkin V.I., Medvedev A.V. Study of dynamic processes in the ionosphere during interval of low solar activity from data of radio physical complex of ISTP SB RAS. The proceedings "Actual problems in remote sensing of the Earth from space". V.8. No.4. 2011.

Contact G. Zherebtsov
(uzel@iszf.irk.ru)

Analyses of the ionospheric disturbance layer during solar activity decreasing

Regular continuous measurements by Irkutsk ionosonde DPS-4 for vertical sounding were automatically treated and the level of ionospheric disturbance was analyzed. Electron density variations during 2004-2009 (declining phase of the solar activity) were studied in details. A spectral criteria was used for finding ionospheric disturbances with periods of 1 to 6 hours corresponding to internal gravitational waves.

It was revealed that in the daytime a number of wave disturbances decrease with solar activity diminishing, while at the night time there is no direct connection between disturbances and the value of F10.7 index.

Seasonal distribution of the amount of wave disturbances shows that the largest number of disturbances is observed in winter, but in the daytime there is a local spring maximum in the distribution.

Complete analyses of the long-lasting continuous data sets from the ionosonde gives additional possibility to robotize the process of searching the most powerful wave disturbances for detailed study of their altitudinal-temporal structure and motion properties using LFM-ionosonde and radar in Irkutsk.

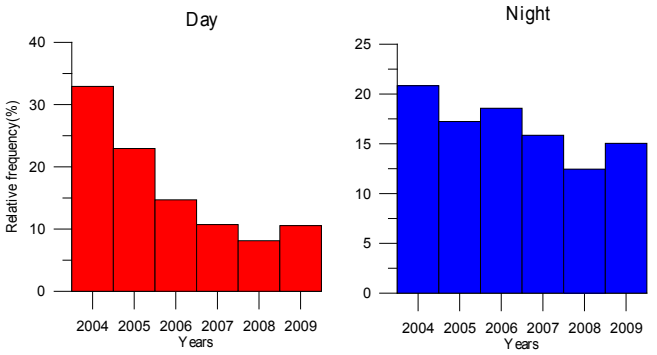

A total number of wave disturbances during declining phase of solar activity in 2004-2009.

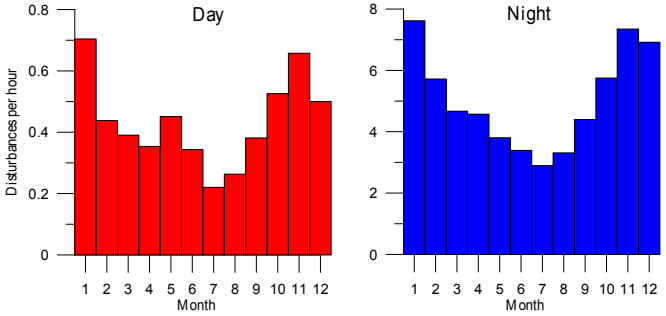

Seasonal distribution of wave disturbances during declining phase of solar activity in 2004-2009.

Zherebtsov G.A., Kurkin V.I., Medvedev A.V. Study of dynamic processes in the ionosphere during interval of low solar activity from data of radio physical complex of ISTP SB RAS. The proceedings "Actual problems in remote sensing of the Earth from space". V.8. No.4. 2011.

Contact G. Zherebtsov
(uzel@iszf.irk.ru)

Variability of the F2-layer parameters for the quiet midlatitude ionosphere under low solar activity

Analysis of statistical properties of variability of the *F*2-layer maximum parameters (the critical frequency *foF*2 and the height *hmF*2) of the quiet midlatitude ionosphere under low solar activity in the daytime (10-15 LT) and nighttime (22-03 LT) hours on the basis of Irkutsk station data for 2007-2008 made it possible to state that:

1. The distribution density of $\delta foF2 = (foF2/foF2_m - 1)100\%$, where $foF2_m$ is the quiet median, can be presented as consisting of two distinctly different normal distributions, one of which corresponds to weak ($|\delta foF2| < 10\%$) and the other to strong ($30\% > |\delta foF2| > 10\%$) fluctuations in *foF*2 (Figure).

The weak fluctuations of *foF*2 to a substantial degree are related to the ionospheric variability at times within 1-3 h and are caused mainly by the internal gravity waves in the atmosphere. The strong fluctuations of *foF*2 are mainly related to day-to-day variability of the ionosphere at a fixed local time and are associated with the ionospheric effects of the planetary waves and tides.

Very strong ($|\delta foF2| > 30\%$) fluctuations of *foF2* occur very seldom (approximately in 1% of cases) and mainly at night. They do not follow normal distribution, and almost all of them are positive ($\delta foF2 > 0$).

2. The distribution density of $\Delta hmF2$ is close to the normal distribution both in daytime and nighttime (Figure). This density can be approximated by a single normal law because the *hmF2* fluctuations within 1-3 h contribute significantly both to the weak and strong *hmF2* fluctuations both by day and at night.

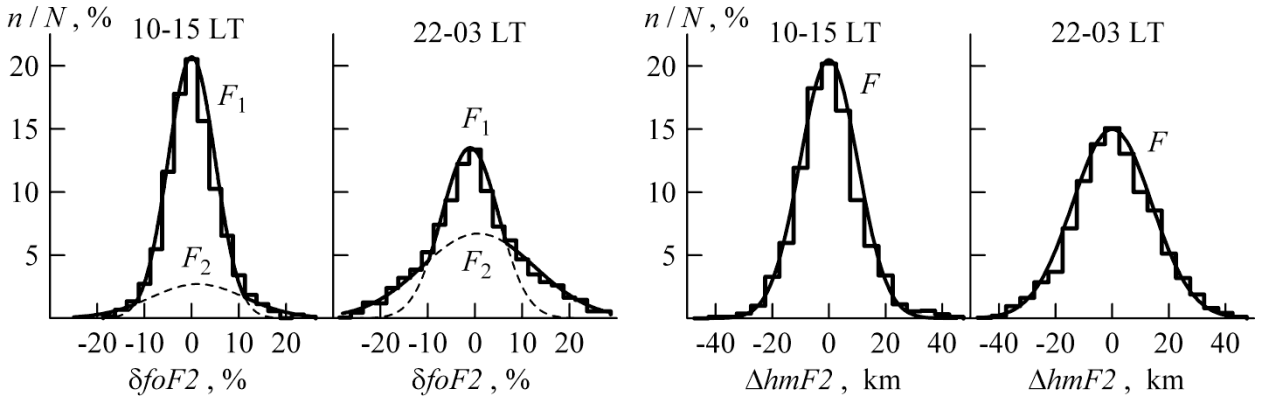

Histograms of $\delta foF2$ and $\Delta hmF2$ for the daytime (10-15 LT) and nighttime (22-03 LT) hours and their approximation by the normal distributions: F_1 and F_2 for $\delta foF2$ and F for $\Delta hmF2$.

Deminov, M.G., Deminova, G.F., Zherebtsov, G.A., Pirog, O.M., Polekh, N.M. Variability of parameters of the F2-layer maximum in the quiet midlatitude ionosphere under low solar activity, Geomagn. Aeron., 51 (3), 348-363, 2011

Contact M. Deminov
(deminov@izmiran.ru)

Diurnal, spectral and dynamic characteristics of medium-scale traveling ionospheric disturbances.

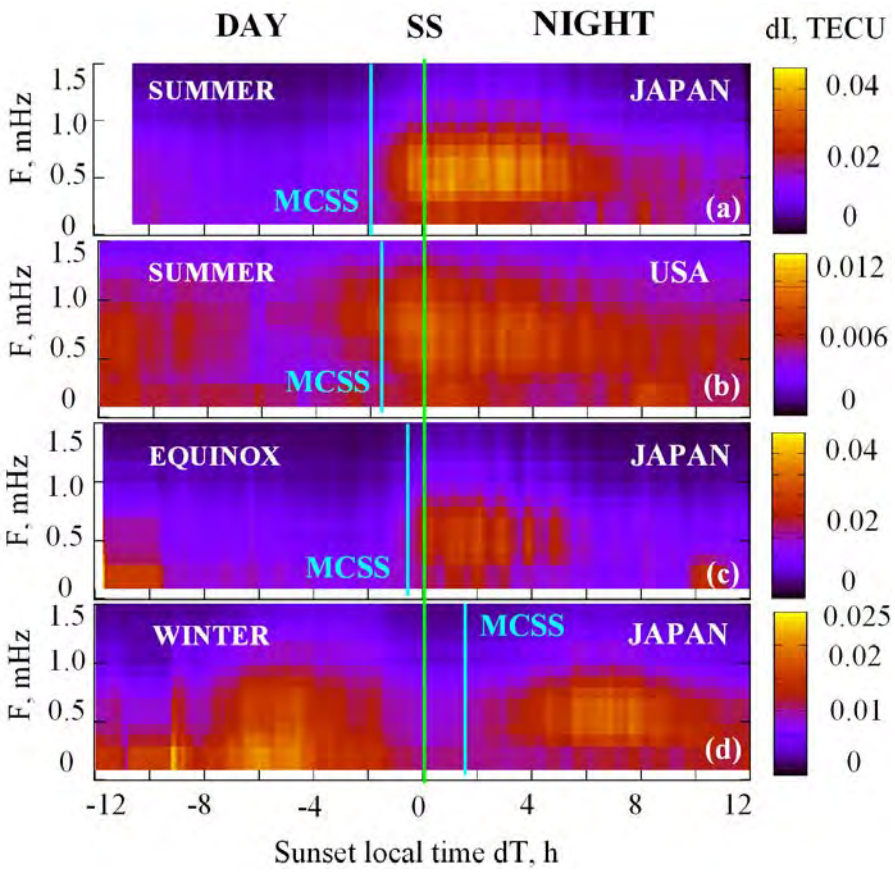

It has been shown for the first time that diurnal, spectral and dynamic characteristics of medium-scale traveling ionospheric disturbances (MS TID) depend on the solar terminator (ST) position (not only at the observational point, but in a magneto conjugate region as well).

In summer, in the Northern hemisphere, MS TIDs are registered 1.5-2 hours before the appearance of the evening ST at an observation point and at the moment of the ST passage through the magnetoconjugate region (Fig. 3a–b). In winter, MS TIDs are observed mostly in 3 hours after the evening ST passage (Fig. 3d).

The periods of observed oscillations correspond to those of the first harmonics of stationary slow magnetoacoustic (SMA) waves propagating along geomagnetic field lines (~103–104 s). The results provide support for the ISTP-developed model of SMA propagating in the internal magnetospheric resonator.

Contact A.S.Leonovich
(leon@iszf.irk.ru)

E.L. Afraimovich, I.K. Edemskiy, A.S. Leonovich, L.A. Leonovich, S.V. Voeykov, Yu.V. Yasyukevich. The MHD nature of night-time MSTIDs excited by the solar terminator, Geophys. Res. Lett., 36, L15106, doi:10.1029/2009GL039803.36.

Ionospheric response to solar eclipse on 1 Aug. 2008 observed by radio wave back-scattering due to natural ionospheric disturbances (partial reflections) and artificial periodic irregularities (API).

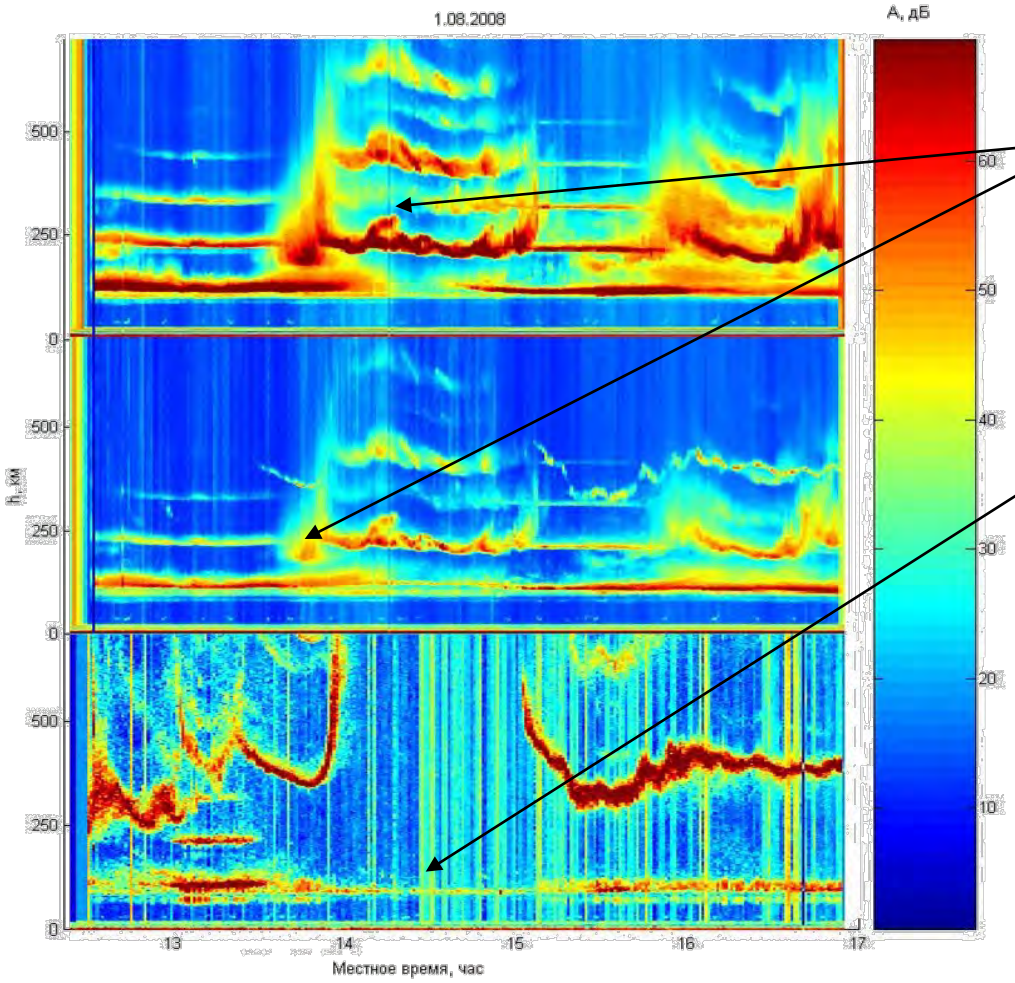

During the solar eclipse (1 August 2008: start 13:07; max 14:16; end 15:22) partial reflections change, radio emission of 4.7 MHz is no longer reflects from the ionosphere and the API disappeared.

Measurements of partial reflections were used to determine the **electron density** in the ionospheric D-layer, which **decrease significantly during the eclipse**.

Contact V.L. Frolov
(frolov.418@nirfi.sci-nnov.ru)

Characteristics of the equatorial F3 layer from the Intercosmos-19 data.

Characteristics of the equatorial *F*3 layer on the base of unique data set of the Intercosmos-19 satellite for the high solar activity (~3600 orbits, 1979-1981) are investigated.

*F*3 layer manifests itself as a cusp in the topside ionogram (Fig.1).

The diurnal, seasonal, latitudinal and longitudinal variations in *F*3 occurrence probability *P*, diurnal variations in *hmF*3 and latitudinal variations in *foF*3 are revealed. *F*3 layer starts to build up coupled with the equatorial anomaly (EA) at ~08 LT. *F*3 layer occurrence probability in the interval from 12 LT to 22 LT averages 40-45% independently of a season. The occurrence probability decreases towards morning, as a consequence *F*3 layer does not appear at 05-07 LT. Three local peaks in *P* connected with the equatorial vertical plasma drift appear in the diurnal variations for all seasons: at 12-14 LT, 17-18 LT and 20-22 LT. The *F*3 layer height over the equator increases from ~450 km in the early morning to 600-750 km in afternoon and up to 950 km in the late evening. The seasonal variations in *P* are weak. *F*3 layer builds up between the EA crests usually on the latitudinal interval ±10°*I*, this interval increases up to ±25°*I* when EA develops strongly. *F*3 layer is usually located symmetrically around the magnetic equator. Longitudinal variations as well as diurnal variations in *P* depend on longitudinal variations in the EA structure which are mainly determined by the variations in the equatorial vertical plasma drift. They are described recently by “wave 4” conception but the Intercosmos-19 data cast some suspicion on this conception. The longitudinal-latitudinal *F*3 layer distribution (on the left) and the occurrence probability *P* dependence on latitude (on the right) for the summer solstice are shown as examples in Fig.2.

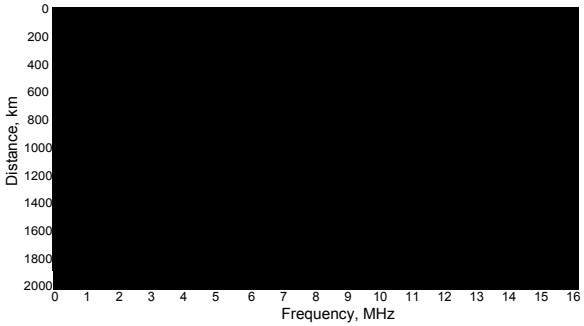

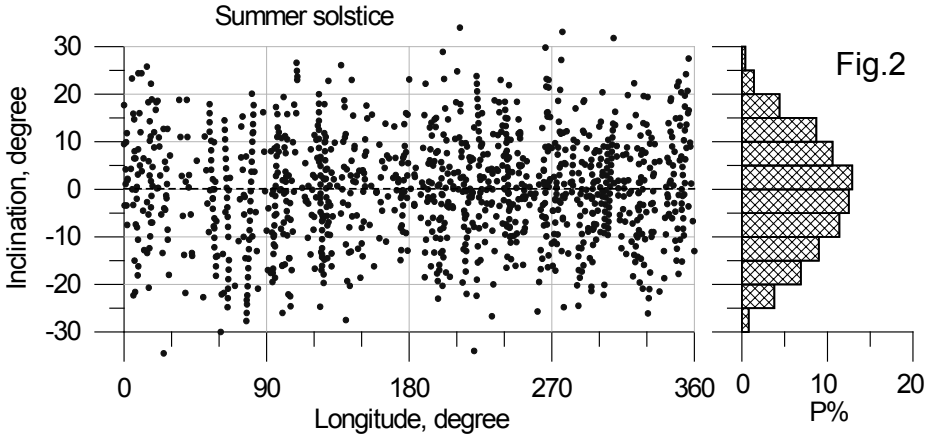

Fig.2

Karpachev A.T. et al., Equatorial F3-layer from the Intercosmos-19 satellite data, JASTP, in press.

Contact A.Karpachev (karp@izmiran.ru)

The effect of liquid-propellant rocket engines (LPRE) of the cargo transportation vehicle (CTV) “Progress” on the surrounding ionosphere.

Space experiments “Plasma-Progress” (September 2007, February and September 2008, February and September 2009) involved measurements of parameters (reflecting characteristics, sizes, density, etc.) of large-scale plasma formations produced by LPRE functioning onboard CTV “Progress” with different directions of exhausting plumes relative to the CTV motion.
With the use of the ISTP SB RAS Incoherent Scatter Radar, it is revealed that in the surrounding ionosphere, a low electron density area (20–40% less than the background value, lifetime is 10–15 min) is formed after a short thruster firing (5 sec).

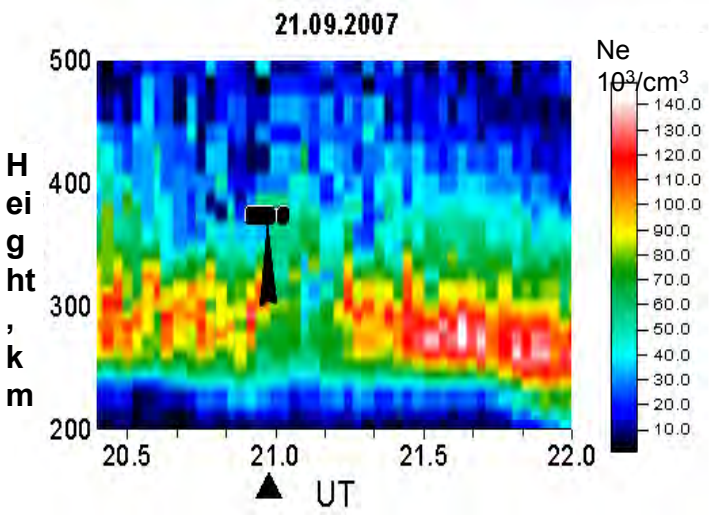

Dynamics of the formation of low electron density area after the thruster firing (▲). Position of the cargo transportation vehicle and thruster plume is shown.

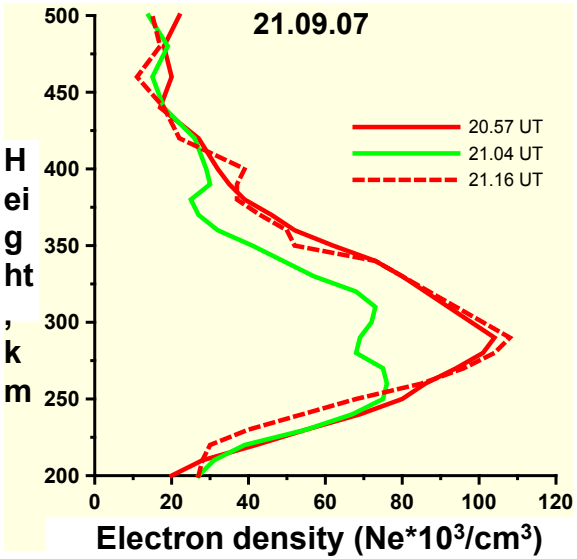

Electron concentration profiles: the background (—), disturbed (—) and recovered (- -) ionosphere.

Contact A.V. Medvedev (medvedev@iszf.irk.ru)

4. THE EARTH'S ATMOSPHERE

Anomalous high values of 557.7 nm mid-latitude airglow intensity during periods of winter sudden stratospheric warmings in Eastern Siberian region

Anomalous high values of 557.7 nm airglow intensity can be caused by high level of mean intensity of this emission in winter months in the period of high solar activity. During sudden stratospheric warmings (SSW), variations with the periods about several days superpose on the mean level of 557.7 nm airglow intensity, providing anomalous high diurnal values of this airglow at the peaks. High airglow intensity in winter months in Eastern Siberia may be connected with 2-3 times increasing of atomic oxygen density at the emitting heights of 85-115 km during periods of high solar activity. The received results are in good agreement with the atomic oxygen density variations measured at high latitudes in Eastern Siberia (Yakutsk) during the 23-rd solar cycle.

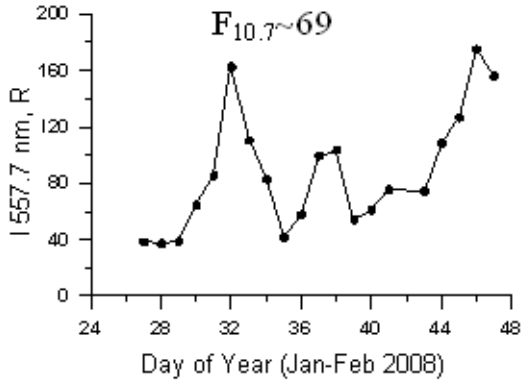

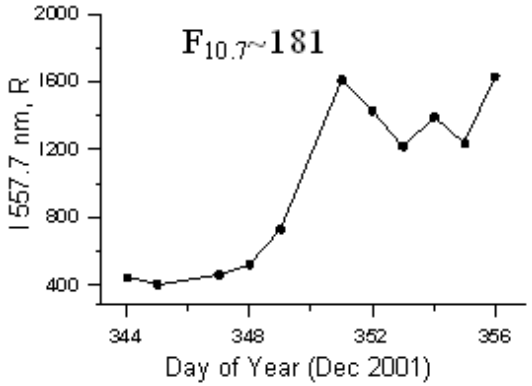

Diurnal variations of 557.7 airglow during SSW periods at 2 levels of solar activity. Annual values of F10.7 index are specified.

Contact V.I. Kurkin (kurkin@iszf.irk.ru)

3D Numerical simulations of ozone response to geomagnetic storms

The response of atmospheric chemical composition in both polar regions was studied with CAO-3D photochemical-transport model for the middle atmosphere (*Krivolutsky et al., 2006)*. Relativistic electrons precipitating from radiation belts during geomagnetic storms and solar protons can penetrate below 100 km into the polar atmosphere sometimes reaching the stratospheric levels loosing energy and causing strong ionization (each 35 eV gives one pair of ions). This leads to additional production chemical compounds which destroy ozone by chemical catalytic cycles.

Photochemical simulations for geomagnetic storms in October - November 2003 show strong ozone depletion over both polar region. Nevertheless, Northern and Southern polar regions response differently mostly due to two factors: polar cap expansion during the geomagnetic storm and the effect of horizontal transport. The results of photochemical simulations generally agree with satellite observations.

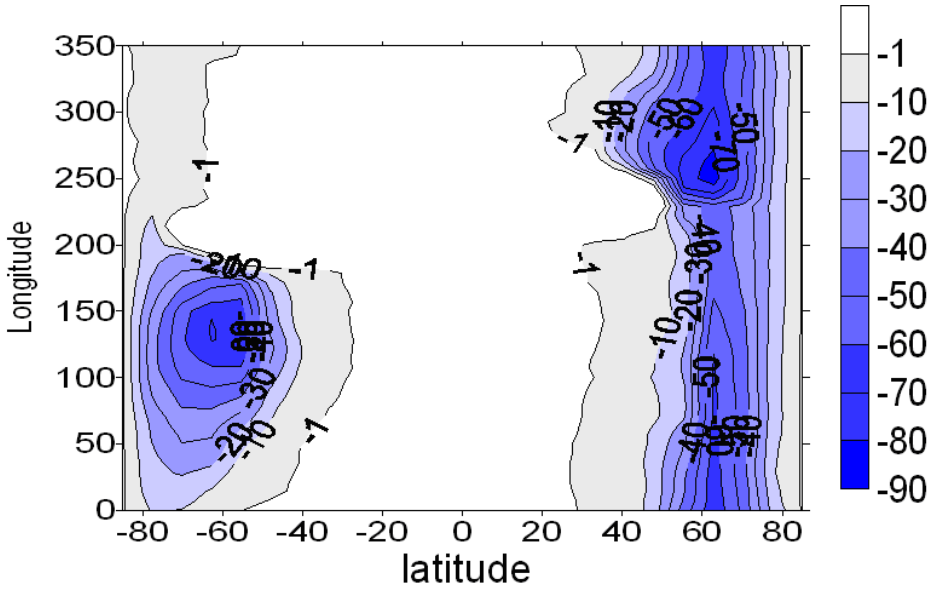

Global ozone response (%) at 66 km height to energetic particle fluxes as simulated with 3D photochemical model for 28 October 2003.

Contact A.A. Krivolutsky
(alexei.krivolutsky@rambler.ru)

Impact of meteorological parameters on the lower ionosphere from LF-VLF monitoring

3-year monitoring of LF – VLF signals from radio stations in the mid-latitude ionosphere located at distances up to 2000 km from the receiver (Michnevo, 54.94°N, 37.73°E) showed that during quiet Sun in the absence of geomagnetic disturbances, the lower ionosphere is significantly disturbed by the dynamical processes in the middle atmosphere. Simulations using EOS-Aura data and plasmochemical model are in a good agreement with observational data. Clear signatures of atmospheric wave processes are detected in the spectra of VLF-LF signals. Composite analysis of VLF-LF and EOS-Aura data has confirmed SAVNET results and shown that the periods of strong temperature and water content disturbance correlate with the sweep of dynamical bifurcation process in the radiowave propagation.

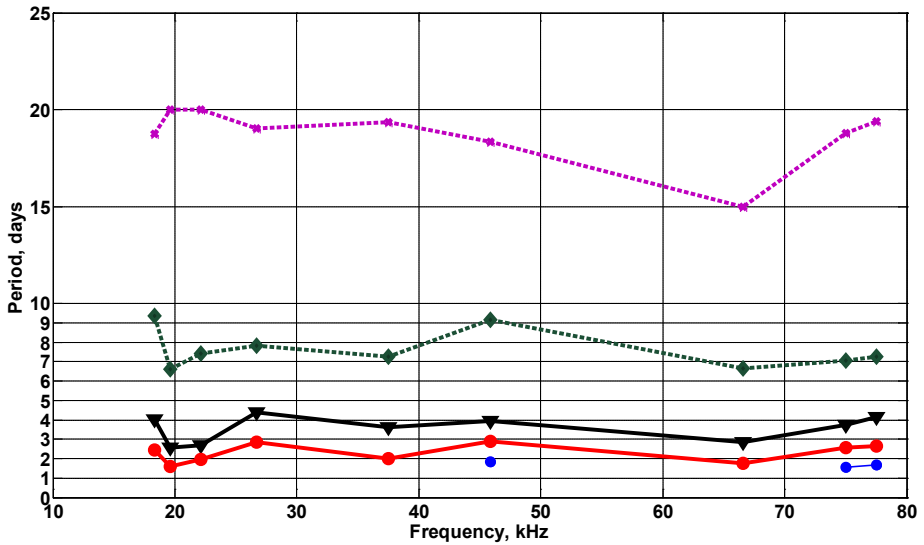

Statistically significant periods observed in the time series of VLF-LF signals over Europe.

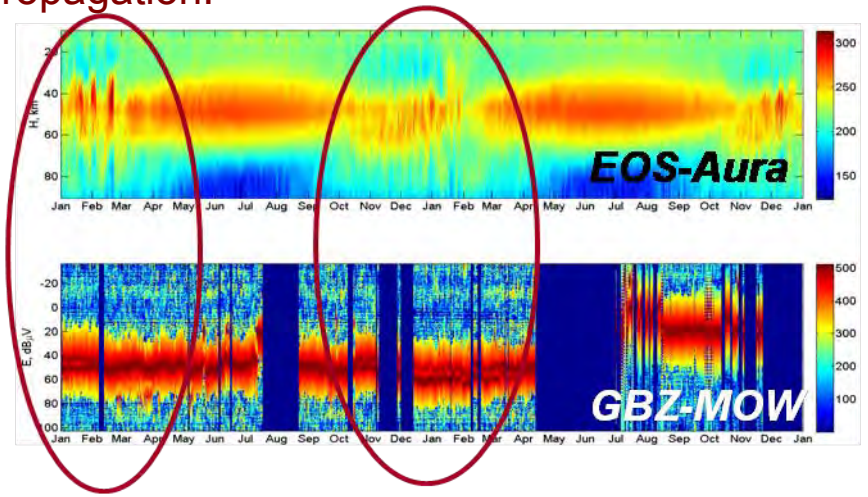

Bimodality of VLF amplitude PDF under temperature jerks in middle atmosphere

Contact Yu.I. Zetzer
(zetzer@idg.chph.ras.ru)

Dynamics of lidar reflections in the ionosphere

Dynamics of lidar reflections in the ionosphere is investigated. The correlation of 532 nm lidar signals scattered on heights of 150-300 km with parameters determining the plasma state in the night ionospheric F2 layer and with the fluxes of charged particles is revealed. It is shown that such signals are possibility formed as a result of light scattering on Rydberg atoms, originating from magnetospheric soft electron precipitations during geomagnetic disturbances.

The formation of aerosol layers is observed at a height of 60-75 km during stratospheric warmings and simultaneous temperature decreasing in the area under the mesopause and an increase of relativistic electron fluxes with energies 92-526 kev at a height of 660 km.

Bychkov V.V., Perejogin A.S., Shevtsov B.M., Marichev V.N., Matvienko G.G., Belov A.S. Lidar observations of appearance aerosol in the middle atmosphere of Kamchatka in 2007-2011. Optics of Atmosphere and Ocean. 2011. V.24. No.12.

Contact B.M. Shevtsov
(bshev@ikir.ru)

Software for intellectual analysis of ionospheric and geomagnetic data

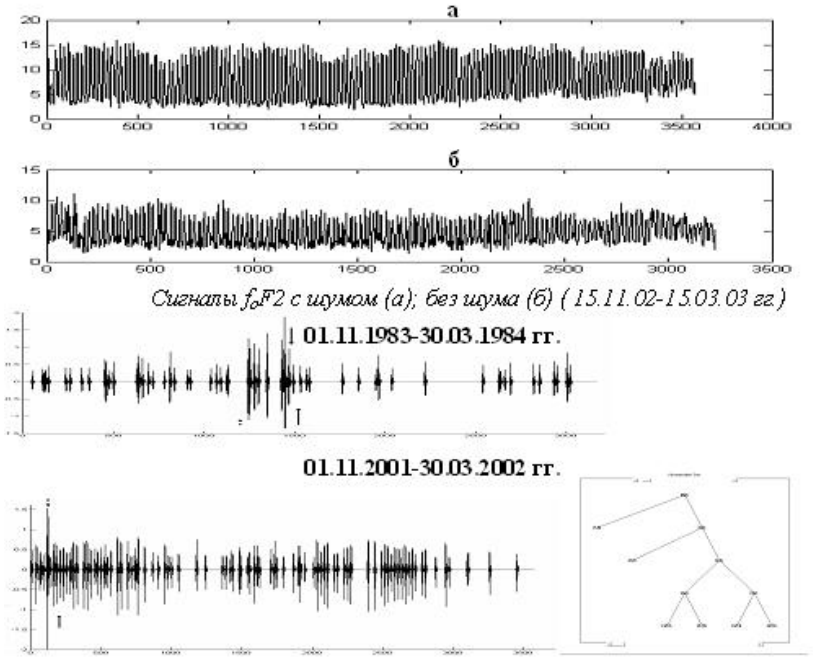

The components of the signal of critical frequency f_0F2: a- with the noise, b –without noise. The analyzing components are represented as wavelet-packet on the right

On the basis of wavelet - technologies a complex of numeral algorithms and software for analysis of ionospheric and geomagnetic data is developed. This complex provides separation and classification of characteristic structures and anomalous features connected to solar and seismic activities, and it also enforces effective wavelet noise suppression. The multicomponent model for a signal of critical frequency f_0F2 is constructed, the latent regularities in the structure of the signal are revealed, the isolated features preceding the increase of geomagnetic activity are marked.

Mandrikova O.V., Solov·ev I.S. Wavelet-technology of the processing and analysis of the variations of Earth's magnetic field . Information Technologies 2010 г. №12. P.37- 44

Contact V.B. Bulgakova (vbulg@ikir.ru)

Approaches to the decision of problems of influence of space and terrestrial weather on people health

The input data set is a multidimensional time serious of daily measurements of arterial blood pressure and disease of a myocardial infarction in clinics of Moscow.
It was established that among the factors concerning myocardial infarctions the greatest influence has atmospheric pressure.

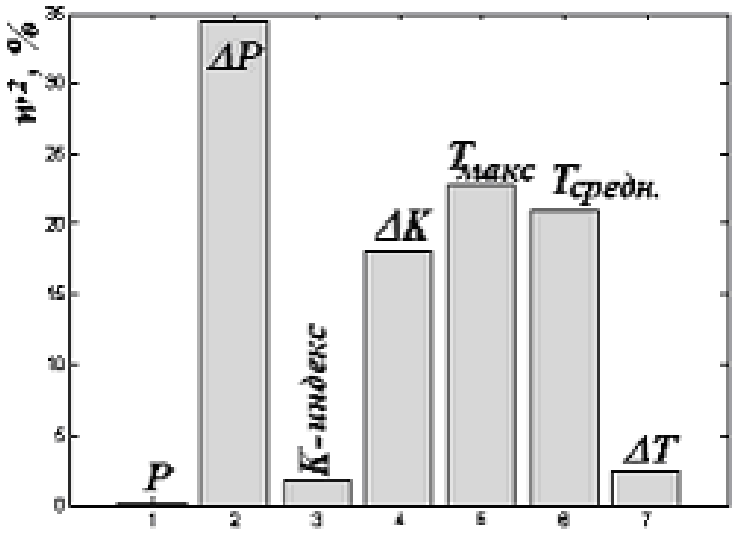

Relative biotropy of atmospheric pressure, jump of atmospheric pressure in relation to a previous day, the K-index, K-index jump in relation to a previous day, the maximum temperature for a day, daily average of temperature and temperature jump in relation to previous day.

V. A. Ozheredov, T. K. Breus, Yu. I. Gurfinkel, b, D. A. Revich, and T. A. Mitrofanova, Influence of Some Weather Factors and Geomagnetic Activity on the Development of Severe Cardiological Pathologies, Biophysics, 2010, Vol. 55, No. 1, pp. 110–119.

Contact T.K. Breus (breus36@mail.ru)